NUMERICAL SIMULATION OF FLUID FLOW AND HEAT TRANSFER IN A THIN LIQUID FILM OVER A STATIONARY AND ROTATING DISK AND COMPARISON WITH EXPERIMENTAL DATA

by

Amir Faghri, Ph.D.
Brage Golding Distinguished Professor
Department of Mechanical and Materials Engineering
Wright State University
Dayton, OH 45435

and

Theodore D. Swanson, P.E.
Thermal Management Group
NASA Goddard Space Flight Center
Greenbelt, Maryland 20771

TABLE OF CONTENTS

NOMENCLATURE

c_f Friction coefficient, $\tau_w/(0.5\ \rho W^2)$

F Nondimensional velocity in radial direction (equation 2.11)

Fr Froude number, $W/\sqrt{g\delta}$

$\vec{g}$ Gravitational acceleration, $-\ 9.81\ \vec{j}\ m/s^2$

G Nondimensional velocity in angular direction (equation 2.12)

h Convective heat transfer coefficient, W/m^2K,

$$= \begin{cases} q_w/(T_w - T_b), & \text{for heating} \\ q_w/(T_w - T_{sat}), & \text{for evaporation} \end{cases}$$

$\vec{i}$ Unit vector in angular direction

$\vec{j}$ Unit vector in the direction normal to the plate

k Cell index in radial direction

K Thermal conductivity, W/mK

$\vec{k}$ Unit vector in z-direction

n Coordinate normal to the free surface, or number of grid cells in radial direction

$\vec{n}$ Unit vector normal to the free surface

Nu Nusselt number, $= h\delta/K$

p Static pressure, Pa

p_o Ambient pressure, Pa

Pr Prandtl number

q Heat flux, W/m^2

Q Volumetric flow rate, m^3/s

Q_{loss} Local rate of volume loss at a cell next to free surface, m^3/s

r Radial coordinate, m

R Radius of curvature

Re Reynolds nubmer, $W\delta/\nu$

t Time, s

$\vec{t}$ Unit vector tangential to the free surface

T Temperature, ^{o}C

u Velocity in angular direction, m/s

v Velocity in the direction normal to the plate, m/s

$\vec{V}$ Velocity vector, m/s

w Velocity in the z-direction, m/s

W_{in} Average radial velocity at entrance, m/s

x Coordinate in angular direction, m

y Coordinate normal to the plate, m

z Coordinate in the radial flow direction (Fig. 1), m

Greek Symbols

α Thermal diffusivity, m^2/s, or relaxation factor

δ Film thickness, m

δ^* Film height corresponding to Fr = 1, m

ζ Nondimensional coordinate perpendicular to the plate (eqn. 10)

ν Kinematic viscosity, m^2/s

ρ Density, kg/m^3

σ Surface tension, N/m

τ Shear stress at wall, N/m^2

$\underline{\underline{\tau}}$ Stress tensor, N/m^2

ω Angular velocity, rad/s

Subscripts

b	Mixed mean (bulk) condition
c	Cartesian components of velocity
e	Free surface
in	Condition at entrance
out	Condition at exit
r	Component in radial direction
sat	saturation condition
w	Condition at solid wall
ϕ	Component in angular direction

SECTION I

FLOW OVER A STATIONARY DISK

1.1 SUMMARY

Improvements in the theoretical model and computational procedure for the prediction of film height and heat-transfer coefficient of the free surface flow of a radially-spreading thin liquid film adjacent to a flat horizontal surface of finite extent are presented. Flows in the presence and absence of gravity are considered. Theoretical results are compared to available experimental data with good agreement. In the presence of gravity, a hydraulic jump is present, isolating the flow into two regimes: supercritical upstream from the jump and subcritical downstream of it. In this situation, the effects of surface tension are important near the outer edge of the disk where the fluid experiences a free fall. A region of flow separation is present just downstream of the jump. In the absence of gravity, no hydraulic jump or separated flow region is present. The variation of the heat-transfer coefficient for flows in the presence and absence of gravity are also presented.

1.2 INTRODUCTION

The radially spreading flow of a thin liquid film is encountered both in the case of axisymmetric discharge of liquid through a thin slot and in the case of impingement of a liquid jet on a solid surface. These configurations are encountered in many engineering devices like spray type heat exchangers, cooling towers, spin coating deposition on metal surfaces, and rotating condensers and evaporators. The appropriate design of these systems require an understanding of the structure of the free surface, the liquid flow field and associated friction and heat-transfer coefficients. These quantities are usually influenced significantly by the magnitude and orientation of the gravitational body force. Therefore, information on these flows in the presence and absence of gravity are required for successful design and operation of these devices on earth as well as in outer space.

One of the earliest works on the radially spreading flow of a thin liquid film was performed by Watson [1]. The film was formed by impingement of a liquid jet on a flat horizontal surface. Both analytical and experimental studies of laminar and turbulent flows were made. A hydraulic jump was found to be present under some flow conditions. The analysis covered the supercritical region before the jump where four different flow regimes were identified and analyzed using the Pohlhausen integral method and a similarity transformation [2]. In the subcritical region, the film height was assumed to be constant. For a given location of the jump, the subcritical height downstream of the jump could be also predicted.

The heat transfer to a thin film formed by an impinging liquid jet was considered by Chaudhury [3], whose analysis basically followed the ideas introduced by Watson [1] except that the energy equation was also solved. In the region away from the impingement location where a similarity solution of the momentum equation was possible, the energy equation was solved in a closed form including the effects of viscous dissipation. An approximate solution for the simultaneously developing hydrodynamic and thermal boundary layers was also obtained using the integral method where the temperature profile was approximated by a fourth-order polynomial.

In a series of studies, Azuma and Hoshino [4] presented the behavior of the radially spreading thin film discharging from a cylindrical gap formed between a circular nozzle and a flat glass plate. Their experimental research determined criteria for laminar-turbulent transition, the liquid film thickness, the velocity profile across the film, stability criteria, and wall pressure fluctuation. The transition from laminar to turbulent flow was established by observing the nature of surface waves with a stroboscope. Several types of waves were identified, and it was proposed that transition occurs when concentric waves change to lattice-shaped waves. This transition depended on the rate of flow, nozzle diameter, discharge gap and radial location. The liquid film thickness was measured with a needle gage. For all the flow rates considered, the film thickness decreased after exit from the nozzle, attained a minimum and increased further downstream. The velocity profile across the thickness of the film was measured using a laser doppler velocimeter. The pressure fluctuation was measured by a pressure transducer which gathered signals from two hypodermic needles embedded on the surface of the disk. Most

experimental measurements were supported by simple theoretical analyses. They identified three regions of the flow: a region just downstream of the nozzle where laminar boundary layer develops but has not reached the free surface, a region where boundary layer reaches the free surface but flow is laminar, and finally a region where flow is turbulent.

Experimental measurements of local heat transfer coefficient when a liquid jet impinges a solid wall and spreads out as thin film was reported by Stevens and Webb [5]. The parameters considered were flow rate, jet diameter and nozzle-to-plate spacing. Correlations for local and average Nusselt numbers were determined in terms of jet Reynolds number. In a later study, Stevens and Webb [6] investigated the effects of jet inclination on the distribution of the local heat-transfer coefficient.

In the abovementioned studies of Azuma and Hoshino [4] and Stevens and Webb [5,6], attention was focused only on the supercritical flow, and no jump was found to be present. A jump is possible when the flow rate is relatively small and disk diameter is relatively large so that transition occurs before the film gets washed out of the disk. Watson [1] and Chaudhury [3] identified the presence of a jump, but their analysis again focused the supercritical region upstream of the jump. A systematic investigation of supercritical and subcritical flows including a hydraulic jump, was carried out by Thomas et al. [7,8] and Rahman et al. [9-11]. In these studies, the film was generated by discharge of liquid through an axisymmetric slot from a pressurized container at the center of the disk.

Thomas et al. [7] numerically predicted the film height variation using a simple one-dimensional model. Neglecting any variation of velocity across the thickness of the film, the continuity and momentum equations were integrated across the thin film to develop a single equation for the film velocity. Results were obtained for both stationary and rotating disks for a number of inlet Reynolds, Froude, and Rossby numbers. In the presence of the jump, the outlet Froude number was always assumed to be unity to simulate a situation where the fluid experiences a free fall over the edge of the disk due to gravity. It was found that the jump moves downstream and may get washed away entirely with an increase in the flow rate, angular velocity and inlet Froude number. Thomas et al. [8] presented experimental data for the liquid film height and a photographic study of surface waves for both stationary and rotating disks. The measurement confirmed the existence of a hydraulic jump for stationary disk which was washed away when the disk was rotated. With the increase of rotational speed, the surface waves changed from wavy-laminar pattern to radial-wave pattern which carried fluid in rivulets on top of a thin liquid sheet adjacent to the disk.

The studies by Rahman et al. [9-11] solved the flow field numerically by a finite-difference method using a boundary-fitted coordinate system. No assumptions regarding the velocity variation or friction coefficient were required. Since the height of the free surface was dependent on the flow conditions and was not known ahead of time, an iterative procedure had to be used to determine the correct location of the free surface. The original method presented by Rahman et al. [9,11] is termed as the 'pressure optimization method'. In this method, the shape of the free

surface was assumed to be described by an algebraic equation with two or more arbitrary constants. The constants were optimized using an exhaustive search technique that minimized the difference between the computed free surface and ambient pressures. When a jump existed in the flow field, the supercritical and subcritical flows were computed separately, and the solutions were matched at the location of the jump. The second method presented by Rahman et al. [10] is termed as the 'porous wall method'. In this method, the free surface is assumed to be a permeable wall through which fluid particles may leave or enter the control volume depending on the difference between the fluid and ambient pressures. The shape of the surface is corrected in successive iterations until the free surface conforms to a streamline and the penetration through the surface reduced to zero. This essentially satisfies the kinematic condition on the free surface. This method computed the whole flow field as a single domain.

The purpose of the present investigation is to critically investigate the merits and drawbacks of the existing computational methods as well as significant improvements for the prediction of thin film flow as discharged from a pressurized vessel at the center of a horizontal stationary disk. The significant improvements sought are assumptions about boundary conditions and inclusion of surface tension at the outlet, an improved iterative procedure for determining the film height, and better criteria for the estimation of error in computed results. Furthermore, the theoretical predictions are also compared with experimental data to establish their validity. The details of the flow structure and heat-transfer coefficient are also determined for flows in the presence and absence of gravity.

1.3 EXPERIMENTAL DATA

The details of the experimental setup and the method of data acquisition and its uncertainty estimates are described by Thomas et al. [8]. Measurements of film height were made for a thin liquid film emanating from a pressurized vessel at the center of a circular horizontal disk. The diameter of the disk was 406.4 mm and the diameter of the collar through which the discharge was made was 101.6 mm. The gap height between the bottom face of the collar and the top of the disk was 0.267 mm, which is also the initial thickness of the discharging liquid film. Water at an average temperature of $22^{o}C$ was used as the test fluid. The closed loop experimental system maintained an isothermal fluid that discharged axisymmetrically on the disk. A noncontact capacitance sensor was used to determine the thickness of the liquid film. The probe was moved along a radius to determine the distribution of film height. The sensing area had a diameter of 11.28 mm, providing reasonably accurate measurements of the film height except for the location of the hydraulic jump. The film height distribution were determined for 5 different flow rates (7, 9, 11, 13, and 15 LPM). Distinct supercritical and subcritical regions isolated by a hydraulic jump were present only for the three lower flow rates. For both 13 LPM and 15 LPM, the subcritical region was washed away from the disk and a partial jump was seen near the outlet. In order to avoid any misleading conclusion, only data for 7, 9, and 11 LPM will be used for comparison with theoretical predictions. Comparison of these experimental data with any theoretical prediction was not attempted in any earlier work, and it is therefore one of the primary objectives of this paper.

1.4 NUMERICAL PREDICTIONS

The radially spreading flow over a stationary horizontal disk of finite extent in the presence and absence of gravity is schematically shown in Fig. 1.1. In the presence of gravity, the flow may encounter a hydraulic jump where incoming supercritical flow transforms to a subcritical flow downstream of the jump. Beyond the disk, the fluid encounters a free fall due to gravity. In the absence of gravity, the flow remains entirely supercritical and no jump is possible. At the exit from the disk, the flow discharges radially. The equations governing the conservation of mass, momentum and energy in a thin liquid layer involving a Newtonian, constant-property liquid can be written as

$$\nabla \cdot \vec{V} = 0 \tag{1.1}$$

$$\frac{D\vec{V}}{Dt} = -\frac{1}{\rho}\nabla p + \nu \nabla^2 \vec{V} + \vec{g} \tag{1.2}$$

$$\frac{DT}{Dt} = a \nabla^2 T \tag{1.3}$$

The boundary conditions are given by:

$$\text{at entrance:} \quad \vec{V} = \vec{V}_{in}, \quad T = T_{in}, \quad \delta = \delta_{in} \tag{1.4}$$

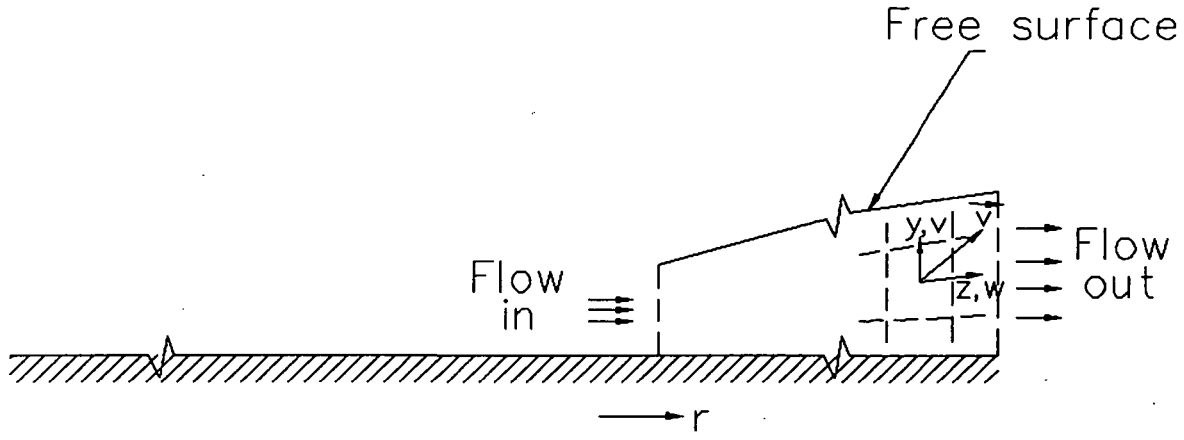

(a) Flow under zero gravity

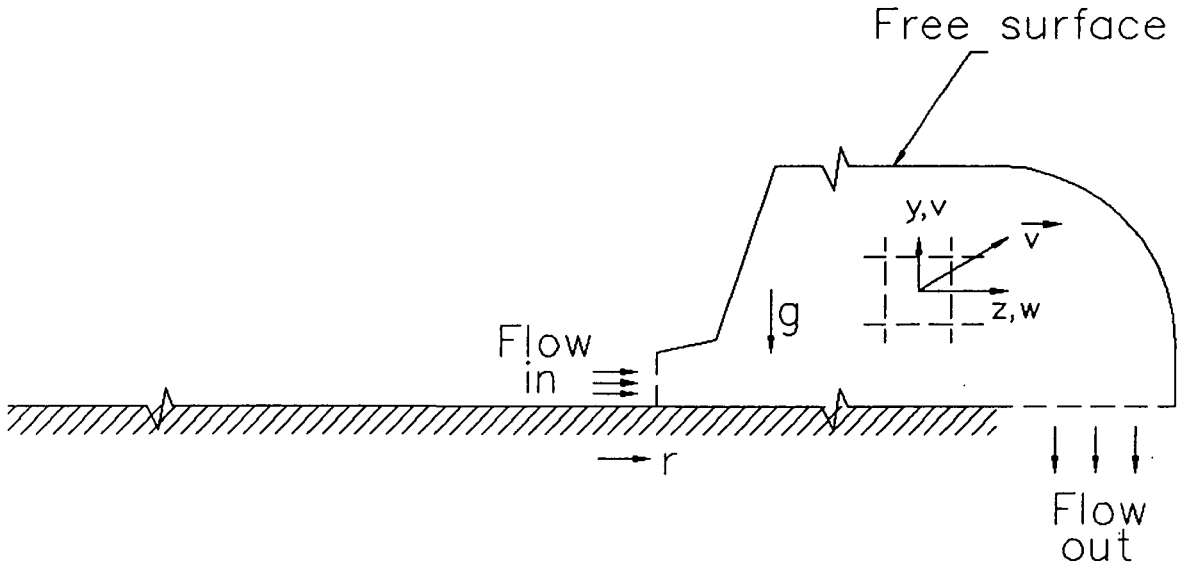

(b) Flow under normal gravity

Fig. 1.1 Schematic of the flow systems and coordinates for computation

at exit:

In the absence of gravity:

$$\frac{\partial \vec{V}}{\partial n} = 0, \quad \frac{\partial T}{\partial n} = 0, \text{ at } r = r_{out} \tag{1.5a}$$

In the presence of gravity

$\delta = \delta_{out}$ (equation 1.11), at $r = r_{out}$

$$\vec{V} = \vec{V}_{out}, \quad \frac{\partial T}{\partial n} = 0, \quad \text{at } y = 0, \quad r_{out} < r < r_e \tag{1.5b}$$

at solid wall: $\vec{V} = 0, \; T = T_w$ (1.6)

at free surface: $\underline{\underline{\tau}} \cdot \vec{n} = 0, \quad \underline{\underline{\tau}} \cdot \vec{t} = 0, \quad \frac{d\delta}{dr} = \frac{v_c}{w_c}, \quad \frac{\partial T}{\partial n} = 0$ (1.7)

Here n is the coordinate directed normal to the surface under consideration. When surface tension is negligible and pressure is the most significant normal stress, the $\underline{\underline{\tau}} \cdot \vec{n}$ condition can be written as $p = p_0$, where 'p_0' is the static pressure of the surrounding medium.

The boundary condition at the exit depends on the existence of the gravitational body force. In the absence of gravity, the flow is entirely supercritical and the film height at the outlet does not need to be specified. In the presence of gravity, when a hydraulic jump is present in the computation domain, a subcritical flow is present in the vicinity of the outlet. Then, the outlet film height need to be specified. In the study of Thomas et al. [7] as well as Rahman et al. [9,10], it was assumed that the Froude number at the outlet ($r = r_{out}$) was unity, since the

subcritical flow becomes critical and finally supercritical as it falls off the disk. Therefore, in the absence of any other better approximation, the flow at $r = r_{out}$ was assumed to be critical. However, in reality, the fluid does not experience the fall until it is swept away from the disk as shown in Fig. 1.1. Moreover, the experimental measurements of Thomas et al. [8] suggests that the flow in the vicinity of the exit is entirely subcritical. Table 1.1 shows a comparison between the experimentally measured film height and the critical height, δ^* predicted by the Fr = 1 condition at the exit. Note that δ^* can be calculated from the continuity equation:

$$\delta^* = \left[\frac{Q}{2\pi\, r_{out} \sqrt{g}} \right]^{2/3} \qquad (1.8)$$

The measured height corresponded to the data point closest to the edge of the disk where measurement was reliable. It appears that the actual film height is about 4 times the critical height. Therefore, even though a free falling condition exists just downstream of exit, the film is held up by some sort of external force.

It can be recalled here that in all previous computations [7,9,10], the surface tension was neglected in all regions of the flow, which may not be correct near the exit since an appreciable curvature of the free surface is encountered due to the rapid turning of the flow. In the presence of surface tension, the fluid and ambient pressures can be related by the equation

Table 1.1: Comparison of the Calculated and Measured Film Height at the Outlet in the Presence of Gravity

Flow rate (LPM)	Measured Height (mm)	Critical Height (δ^*) from eqn. (1.8) (mm)	Deviation of δ^* (%)	Calculated Height (δ_{out}) from eqn. (1.10) (mm)	Deviation of δ_{out} (%)
7	4.420	0.981	-77.81	4.377	-0.95
9	4.318	1.160	-73.15	4.479	3.73
11	4.369	1.337	-69.39	4.582	4.88

$$p_e - p_a = \frac{\sigma}{R} \tag{1.9}$$

where R is the radius of curvature. If the pressure is assumed to be hydrostatic in nature, this equation can be expressed in terms of film height as

$$\delta_{out} = \delta^* + \frac{\sigma}{\rho g R} \tag{1.10}$$

where δ_{out} is the actual film height at the exit end of the disk ($r = r_{out}$), and δ^* is the critical height predicted by the Fr = 1 condition at that location. To solve equation (1.10), an estimate for R is required, since that is unknown in general. The visual observations showed that when the flow changes its direction from horizontal to vertical, the radius of curvature is of the same order as the film height. Substituting $R = 0.5\ \delta_{out}$ and solving for the film height from equation (1.10), we obtain

$$\delta_{out} = \frac{\delta^* + \sqrt{\delta^{*2} + \frac{8\sigma}{\rho g}}}{2} \tag{1.11}$$

Equation (1.11), even though quite approximate in nature, gives a good estimate of film height at $r = r_{out}$. This is also demonstrated in Table 1.1, where the height calculated by equation (1.11) is compared with the measured height. The deviation is within 5% which is reasonable considering the simplicity of formulation. Therefore, whenever a jump was present, the film height at the exit end of the disk was computed from equation (1.11). The liquid film experiences a free fall as it exits from the disk at $r = r_{out}$. Based on the experimental observations and

comparisons seen in Table 1.1, it was assumed that the free surface forms a quarter circular arc with radius R and then extends vertically downward. The radial location of the free surface is given by

$$r_e = r_{out} + 0.5\ \delta_{out}$$

The uniform velocity of the free falling liquid was calculated from the conservation of mass.

The coordinate system used in the present formulation is also shown in Fig. 1.1. the r-axis is directed along the plate radius and y-axis is directed perpendicular to the plate. This r-y system was used for the formulation of the one-dimensional computational scheme where the continuity and momentum equations were integrated across the y-direction. For a complete two-dimensional solution, a body-fitted coordinate system [9] was used. In this system, the coordinates were defined along lines connecting the centers of the adjacent grid cells. The z-axis lies along the main direction of the flow, and the y-axis across the thickness of the liquid layer. Comparing the r-y and z-y system, it can be noticed that the y-axis remains unaltered, whereas the z-coordinate is related to r by a geometrical factor.

The present one-dimensional computational scheme is similar to that developed by Thomas et al. [7] except that the film height at the outlet was calculated using equation (1.11) instead of the critical height. In this scheme the governing equations for mass and momentum (1-2) were integrated assuming a uniform velocity across the thickness of the liquid layer, and were combined to give a single equation for film velocity.

Since the velocity was explicitly specified at r = r_{out}, the free falling flow beyond that location could be ignored. Even though the steady-state solution was desired, the transient term was retained in a simplified form to devise an explicit marching scheme. The friction coefficient, c_f, was estimated using a two-part formulation: Blasius-solution for regions where the thickness of the boundary layer was smaller than the film thickness, and the coefficient obtained from a parabolic velocity profile in regions where the boundary layer encompassed the entire film. The equation was discretized using the MacCormack predictor-corrector method [12]. For each time step, the predicted solution first used forward differencing in both time and space and then improved the prediction using forward differencing in time, but backward differencing in space. The corrected solution was taken as an arithmetic average of the past and predicted solutions. Since the one-dimensional solution did not require a significant amount of computer time, 500 grids were used in r-direction to obtain a smooth distribution of the film height. Convergence to the steady-state solution was obtained within 5000 iterations, where the maximum possible time-step that allowed stability was used.

The complete two-dimensional solution of the flow and temperature fields were performed using a body-fitted curvilinear coordinate system. The grid cells were generated by algebraic interpolation between the boundaries of the computation domain, where the irregular free surface was taken as one of the boundaries. As shown in Fig. 1.1, the local coordinates were defined along lines connecting the centers of the adjacent grid cells. The discretized equations were written for each cell by using principles of conservation of mass, momentum and energy, where the primary

physical variables were retained without any nondimensionalization. The hybrid difference scheme presented by Patankar [13] was used to retain convection and/or diffusion terms. The flow field was solved using the SIMPLEST algorithm as demonstrated by Spalding [14]. The number of grid cells were determined from a series of tests that varied the number of grids in each coordinate direction. It was found that 50 x 30 cells in the z-y plane yielded grid independent solutions and was used for the present computation.

The primary difficulty in two-dimensional computation was that the height of the free surface, which was unknown in general, needed to be specified in order to generate the grid structure and to solve the flow field. Therefore, an iterative procedure was required to ascertain the free surface height distribution. Two possible algorithms, outlined by Rahman et al. [9] and Rahman et al. [10] are 'pressure optimization method (POM)' and 'porous wall method (PWM)', respectively. Here, we would like to suggest improvements for both methods and give advantages of one over the other for certain kinds of problems.

POM is suitable for one-domain flows where no jump is present, and two-domain flows where a jump isolates the supercritical and subcritical flow regimes. In this method, the free surface is approximated by an algebraic equation with a number of arbitrary constants. These constants are optimized by an exhaustive search technique which minimizes the error in the pressure distribution on the free surface defined as

$$\text{Normalized RMS Error} = \frac{\frac{1}{n}\sum_{k=1}^{n} p_k^2}{\rho g\, \delta_{in} + \frac{1}{2}\rho\, W_{in}^2}$$

where p_k is the difference between the free surface and ambient pressures at the kth radial location, and n is the number of cells in the radial direction.

When a jump is present in the computation domain, the film height distribution is computed as follows:

(1) The supercritical film height distribution for the entire disk is calculated by approximating the free surface by the equation
$\delta = \delta_{in}\ ((r - A)/(r_{in} - A))^{an}$.
The parameters 'A' and 'an' are optimized keeping the specified inlet film height constant. This equation allows 2 degrees of freedom. Higher degrees of freedom can be accomodated by assuming more complex forms of the equation. Note that supercritical flow does not require any specification of outlet condition, where the flow is assumed to be locally parabolic in nature.

(2) The subcritical film height distribution for the entire disk is calculated by approximating the free surface by the equation
$\delta = \delta_{out}\ ((r - B)/(r_{out} - B))^{bn}$.
The parameters 'B' and 'bn' are optimized preserving the outlet film height fixed at δ_{out} determined by eqn. (1.11). A free falling condition was present at the outlet.

(3) The jump height distribution corresponding to the supercritical film height distribution is determined from the momentum balance at the jump [15].

$$\frac{\delta_2}{\delta_1} = \frac{1}{2}\left[(1 + 9.6\ Fr_1^2)^2 - 1 \right]$$

where subscripts '1' and '2' indicate conditions upstream and downstream of the jump, respectively.

(4) The location of the jump is determined by matching the jump height with corresponding subcritical film height distribution.

(5) The supercritical film height distribution is recalculated for the partial disk from the entrance to the location of the jump. The method used is the same as that outlined in step (1).

(6) The slope of the jump is determined by calculating the flow as a single domain using the height determined in step (5) for the supercritical region and that from step (2) for the subcritical region. In this process, the jump surface is assumed to form a plane, the location for the initiation of jump is kept constant, and as before, the normalized RMS error is minimized.

(7) The flow and energy equations are solved as a single domain problem using the film height distribution determined in step (6) to find the flow field and heat transfer coefficient.

In steps (1), (2), (5) and (6), the film heights in the different regions are optimized independently to give a minimum normalized RMS error in pressure. The acceptable solution corresponds to a normalized RMS Error

of less than 0.1. This margin was established in [9] from the benchmark problem of falling film flow. Steps (5-7) are improvements over the original POM presented by Rahman et al. [9], in which the jump occurred across one grid cell. So, the extent of the jump decreased with an increase in the number of computational cells. Moreover, the experiments of Thomas et al. [8] suggested a somewhat gradual jump rather than an instantaneous rise in the film height. Step (5) significantly improved the estimation of the film height in the supercritical region. Moreover, in step (2), the free falling flow at the outlet was appropriately modeled and accounted for in the computation of subcritical film height distribution. In the original method [9], the flow at the outlet was always assumed to be locally parabolic with a prescribed hydrostatic pressure gradient. In reality, the flow in a hydraulic jump is elliptic in nature, where outlet conditions significantly affect the location of the jump as well as the film height distribution. In order to accurately determine the heat-transfer coefficient in the vicinity of the jump, the one-domain calculation outlined in step (7) is essential since a natural continuity of the velocity and temperature fields needs to be preserved. It may also be noted that energy equation is solved only after the film height distribution is completely ascertained.

In the PWM, the free surface is assumed to be a permeable wall through which fluid particles are allowed to enter or leave the control volume depending on the difference between the ambient pressure and the pressure in cells next to the free surface. The location of the surface is improved in successive iterations until the rate of penetration becomes negligible. Instead of assigning any particular equation for the free surface height

distribution, the new height is calculated from the old height and the local rate of penetration as shown below.

$$(Q_{loss})_k = Q_{k-1} - Q_k \tag{1.12a}$$

$$(\delta_{corr})_k = \frac{(Q_{loss})_k}{Q_{in}} (\delta_{old})_k \tag{1.12b}$$

$$(\delta_{new})_k = (\delta_{old})_k + a\ (\delta_{corr})_k \tag{1.12c}$$

where a is the relaxation factor. A value of $a = 1$ was found to be adequate for the problems considered here. The apparent advantage of this procedure is that there are more degrees of freedom for the free surface height distribution. The number of degrees of freedom here is the same as the number of grid cells in the radial direction. This technique is also more systematic and uniformly convergent than the exhaustive search technique associated with the POM. The deviation from the ideal zero-penetration condition can be estimated by either of the following measures.

(a) Root-sum-square penetration

$$= \frac{\sqrt{\sum_{k=1}^{n} (Q_{loss})_k^2}}{Q_{in}}$$

(b) Absolute sum of penetration

$$= \frac{\sum_{k=1}^{n} |(Q_{loss})_k|}{Q_{in}}$$

(c) Maximum error in flow rate

$$= \frac{|(Q - Q_{in})|_{max}}{Q_{in}}$$

Since the method is uniformly convergent, all these error measures decrease with the number of iterations. In a practical problem, a solution may be acceptable when both root-sum-square penetration and maximum error in flow rate are less than 0.05 and the absolute sum of penetration is less than 0.1.

The PWM outlined above is significantly different from the method originally proposed by Rahman et al. [10]. In the original method, the correction to the film height was obtained from the kinematic condition on the free surface instead of the local rate of penetration. This improved the surface in successive iterations to form a streamline, but apparently without a significant reduction in the local rate of penetration. Therefore, the convergence was extremely slow. Moreover, frequent smoothing was required to eliminate undesirable irregularities. These drawbacks were removed in the present modified algorithm. There is also a great improvement in the estimation of error. The criteria used by Rahman et al. [10] is RMS penetration, which is somewhat similar to the root-sum-square penetration except that an average was taken over all the cells in the radial direction. The disadvantage of using the average

penetration is that for a given free surface, it can be reduced by making the cell size smaller or increasing the number of cells in radial direction, which is somewhat misleading. In the present investigation, the total penetration over the entire free surface was considered, which was independent of the number of grid cells. Some limitations of the PWM were also discovered. It appears that the method does not work very well when a hydraulic jump is present, since a relatively large influx of fluid is encountered in the vicinity of the jump which leads to incorrect estimates of the subcritical film height downstream of the jump. However, it yields very good results when the flow is entirely supercritical, like flow in a zero-gravity environment.

1.5 RESULTS AND DISCUSSION

The film height distributions for thin film flows over a stationary disk are presented in Figures 1.2-1.4 for flow rates of 7, 9, and 11 LPM, respectively. The inlet height corresponded to the first experimental data point, and the exit height was estimated by using equation (1.11). The two-dimensional solution used the modified POM, where the fluid velocity profile at the entrance was assumed to be parabolic with the maximum at the free surface. In the experiment by Thomas et al. [8], however, the fluid was discharged through a thin slot, so the maximum in the velocity profile at the discharge location is expected to be somewhere between the solid walls. After a short distance from the entrance, the flow is expected to evolve to a parabolic profile with the maximum velocity at the free surface, since the no-slip condition exists on the solid wall and the zero-shear condition is present on the free surface. Therefore, using the first measured data point instead of the physical entrance condition may be

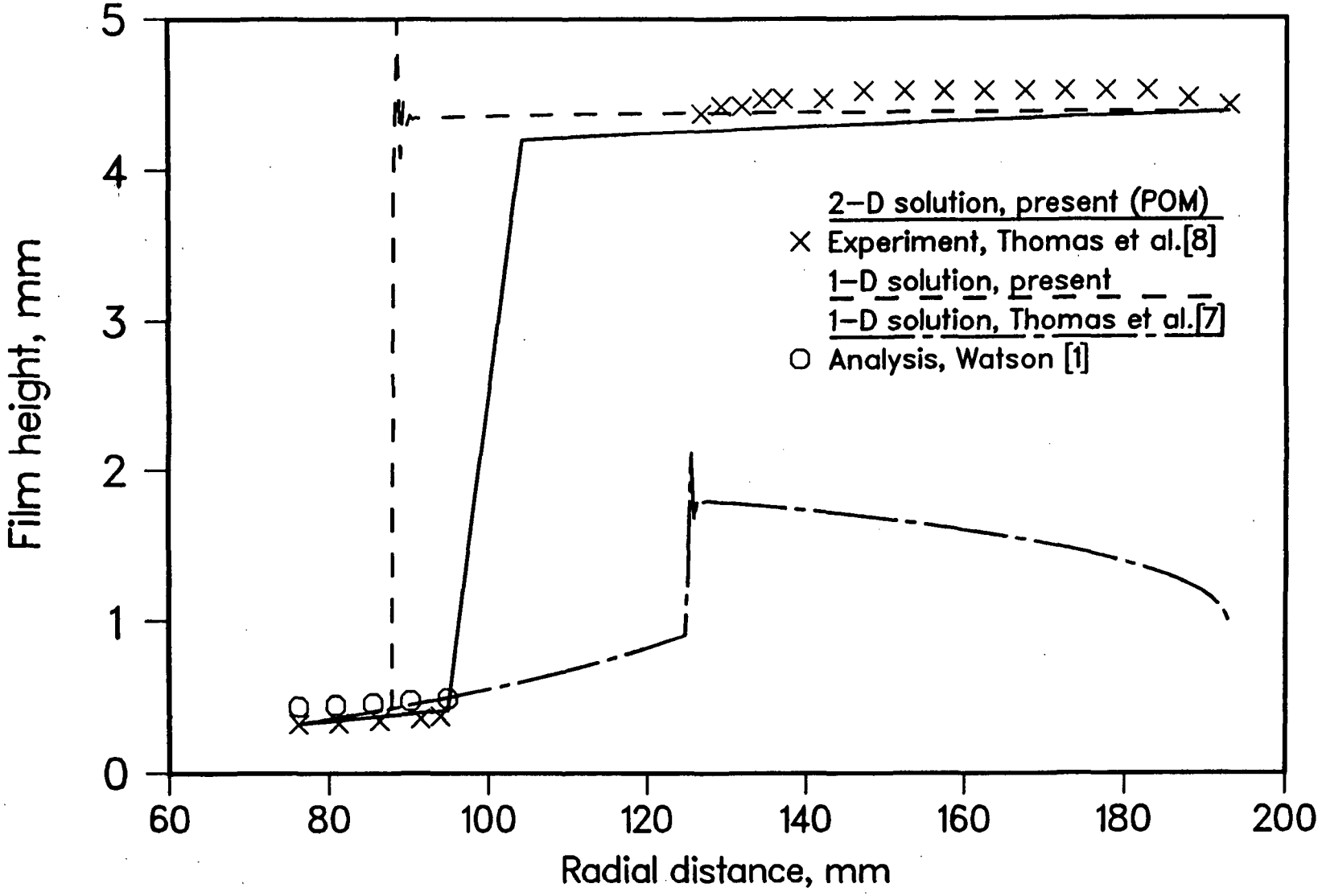

Fig.1.2 Film height distribution for flow under normal gravity at a rate of 7 LPM

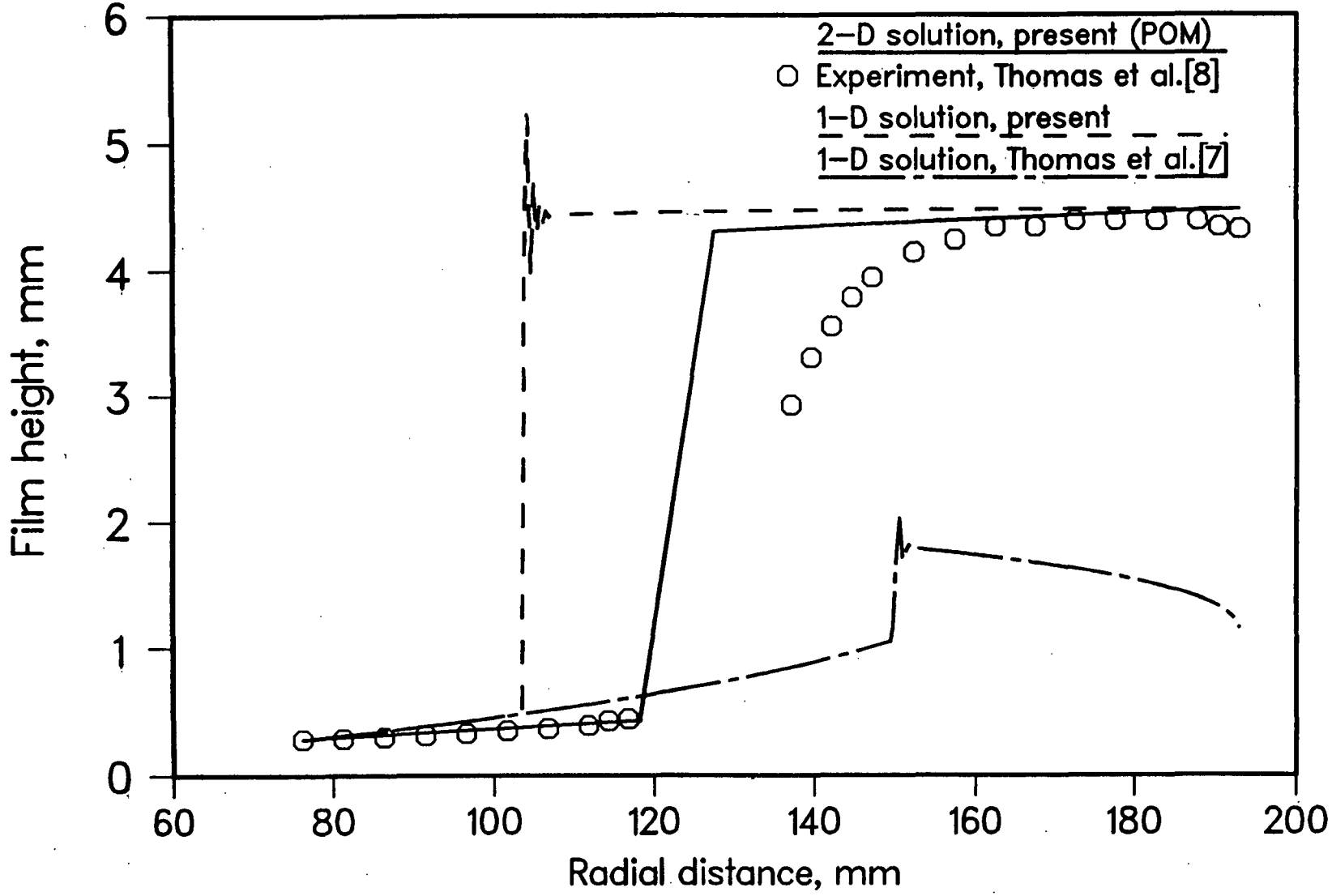

Fig.1.3 Film height distribution for flow under normal gravity at a rate of 9 LPM

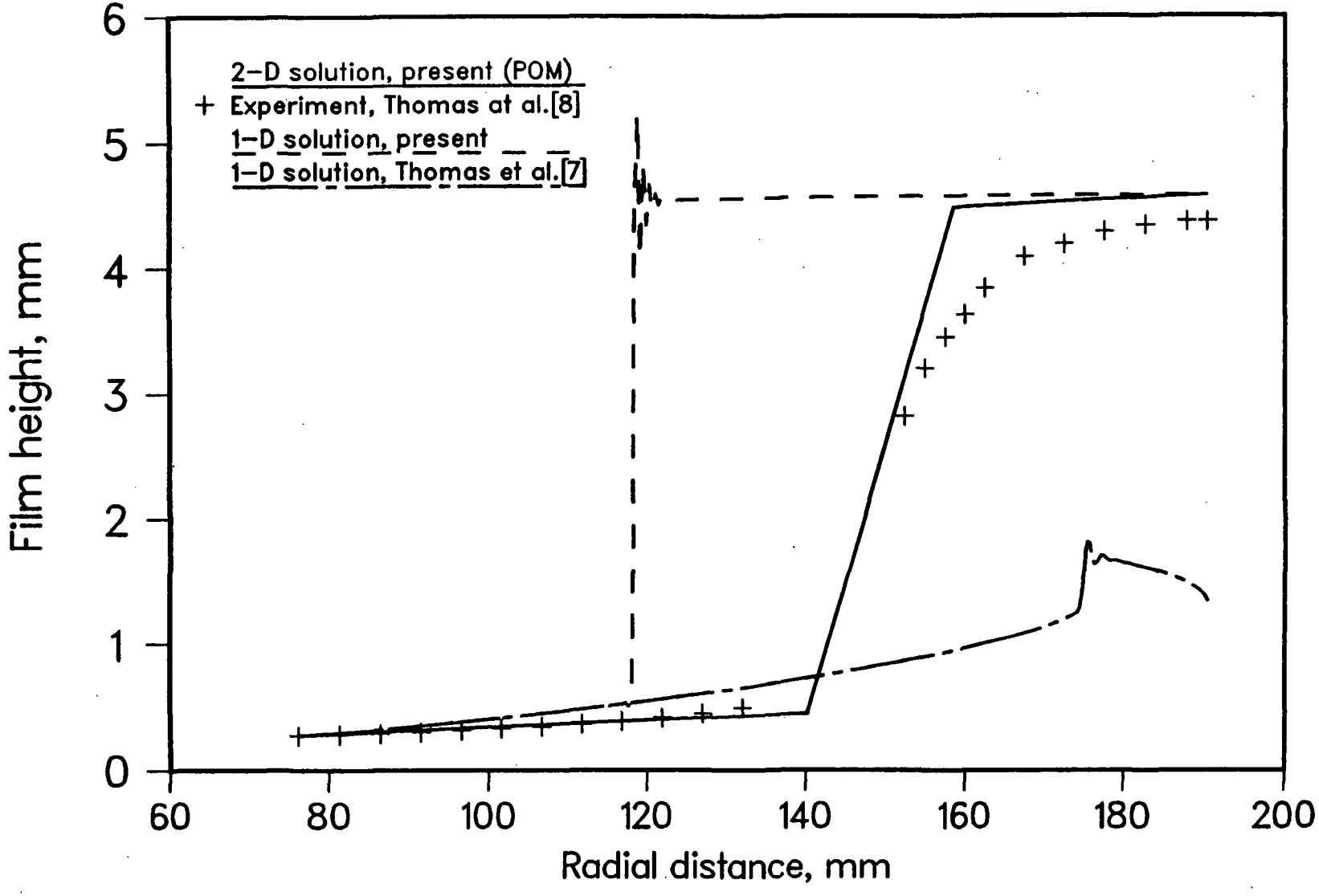

Fig.1.4 Film height distribution for flow under normal gravity at a rate of 11 LPM

more appropriate for the numerical computations.

At all flow rates, the present two-dimensional solution compares best with the experimental measurements. The present one-dimensional solution reasonably predicts the supercritical and subcritical film heights, but the jump appears to occur at a smaller radius. Moreover, the experimental data shows a somewhat gradual jump in contrast to the sudden jump predicted by the one-dimensional solution method. Figures 1.2-1.4 also present a relative comparison of the present results with the one-dimensional solution of Thomas et al. [7] in which a critical condition (Fr=1) was specified at the outlet. The predicted subcritical film height distribution was much lower than that measured experimentally. The distribution of film height in the supercritical region is reasonably close to the experimental data and the two-dimensional solution. The solution of Thomas et al. [7] also predicted that the hydraulic jump occurred further downstream than the experiment. These comparisons show that the POM described above can be an effective mechanism for the prediction of the location of the jump as well as the supercritical and subcritical film height distributions. It may be improved further if the jump is assumed to be a curved surface instead of being a plane, as indicated by the data corresponding to 9 and 11 LPM. This, however, was not attempted here, since the shape of the film at the location of the jump is expected to be quite complicated due to churning motion of the fluid, and since no experimental data were available in regions where the jump is initiated. Figure 1.2 also shows a comparison with the analytical solution of Watson [1] for radially spreading thin film flow initiated by a liquid jet impinging perpendicularly to a solid wall. Since Watson's results depend

on jet radius, an equivalent radius for the present system was calculated as $a_{eq} = \sqrt{2h_c r_c}$, where r_c is the radius and h_c is the thickness of the slot through which the liquid film is discharged. This equivalence was obtained from the relationship between jet radius and film thickness in an invisid flow. Watson's results show a larger film height than that measured experimentally or predicted numerically in the present investigation. The difference may be attributed to the approximate nature of the comparison due to the physical differences of the two flow systems.

The details of the two-dimensional flow field in the presence of gravity is illustrated in Fig. 1.5 for the flow rate of 11 LPM. The velocity profile was parabolic at r = 0.101-0.110 m, which is in the supercritical region. Here the flow is well-structured with the maximum velocity at the free surface. This is the typical velocity profile in most of the supercritical region. However, as the jump is approached and film height increased rapidly, the inertia of the fluid stream decreased to preserve the continuity of fluid motion. Moreover, the stress-free condition on the free surface causes more forward-moving fluid particles to orient themselves to the free surface. Therefore, the flow separates from the solid wall, and a recirculating flow region is seen next to the wall just downstream of the jump. This is the characteristic seen in plots corresponding to r = 0.145-0.154 m and r = 0.174-0.183 m which are in the jump and subcritical regions, respectively. The separation from the solid wall is due to frictional resistance in an adverse pressure gradient and was previously seen in the experimental work of Nakovyakov et al. [16]. They actually measured the wall shear stress for a circular hydraulic jump

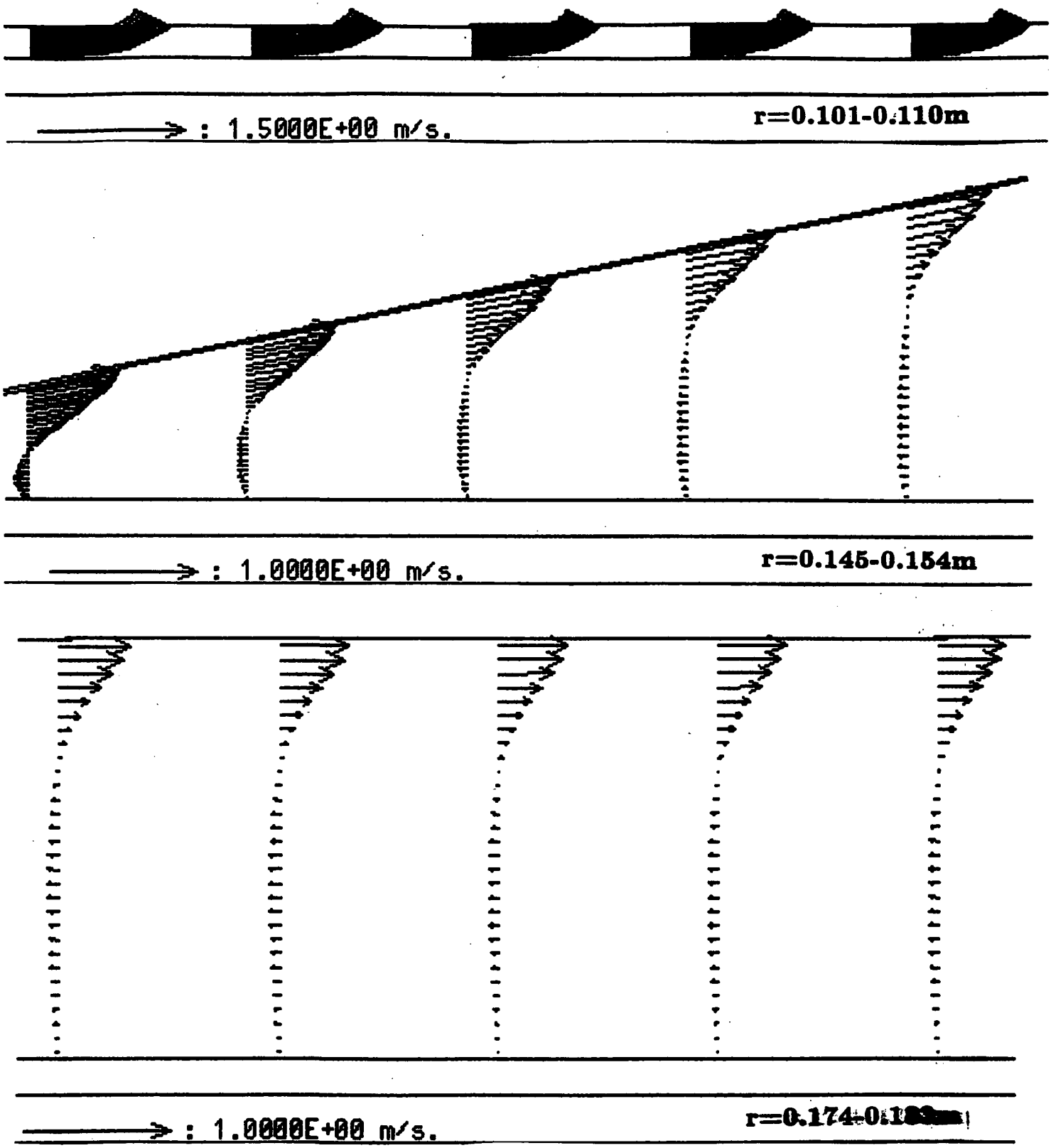

Fig.1.5 Velocity vectors for radially spreading flow under normal gravity at a rate of 11 LPM

of a thin liquid film and found it to be negative for a short distance downstream from the location of the jump.

The friction coefficient becomes zero at the point where the flow separates, and remains negative in the recirculating flow region. In the present work, it was seen that the flow remained separated in the entire subcritical region downstream of the jump. This is due to a relatively small extent of the subcritical region. A test run with a larger radius showed that the flow reattaches to the surface and a parabolic velocity profile is established further downstream. It should be also mentioned here that the above flow structure was obtained for a stationary free surface. The small variation of film height with time due to surface waves was neglected in the numerical computation.

The variation of the film height for radially-spreading flow under zero gravity at a flow rate of 7 and 11 LPM are shown in Figures 1.6 and 1.7, respectively. The dimension of the disk and the entrance flow condition were taken to be the same as the experiment of Thomas et al. [8] and numerical computation presented in Figs. 1.2 and 1.4. Since no experimental data is available for thin film flow in a gravity-free environment, the numerical prediction is the only means to understand the behavior of the flow. In the present work, the PWM was used to iterate the film height distribution, where the root-sum-square penetration and maximum excess flow rate were less than 5 percent, and absolute sum of penetration was less than 10 percent for the final solution. In a zero gravity environment, the film height increases monotonically with distance, and no sudden rise in the form of a hydraulic jump was encountered. Figures 1.6

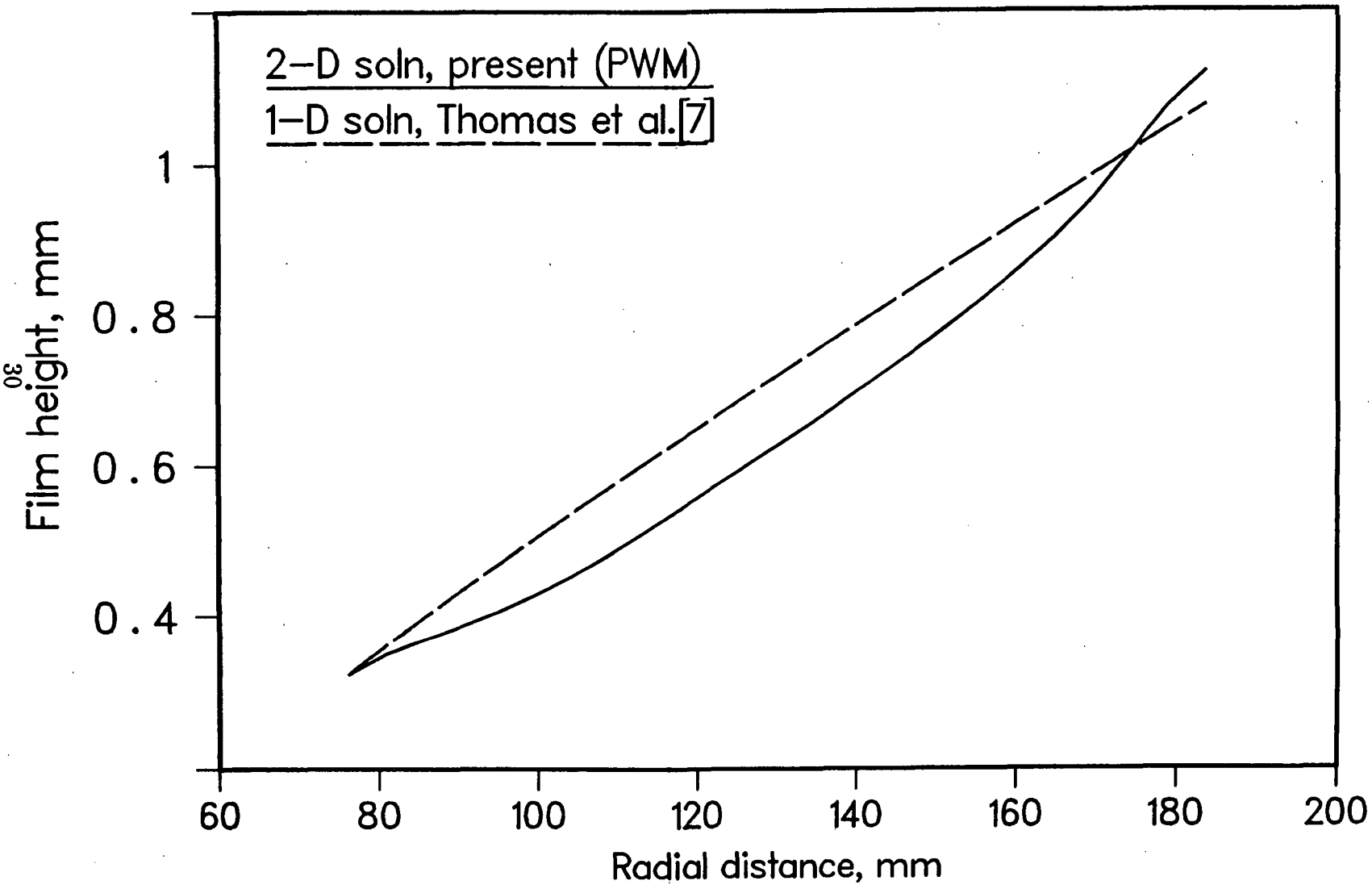

Fig.1.6 Film height distribution for flow under zero gravity at a rate of 7 lpm

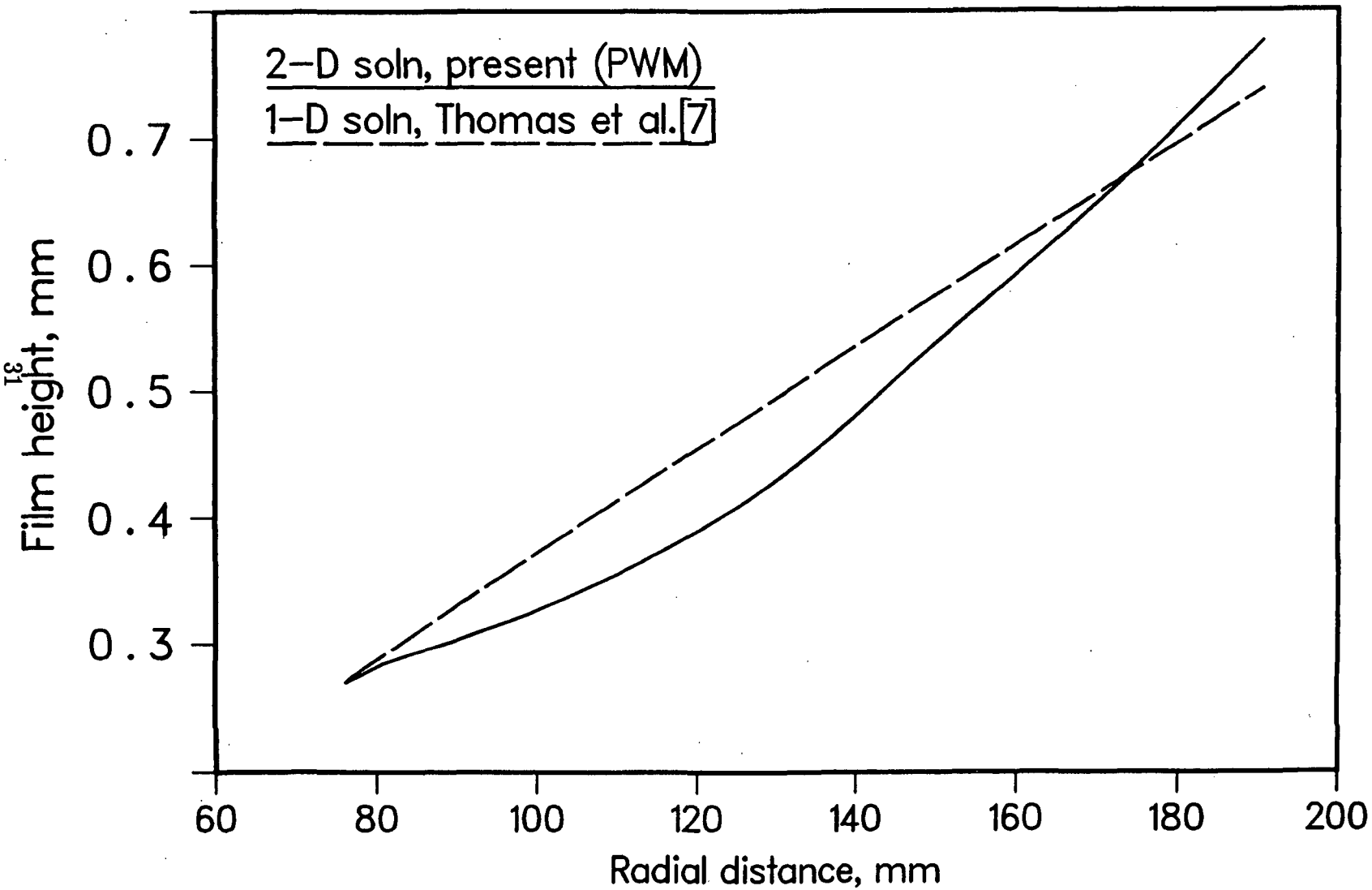

Fig.1.7 Film height distribution for flow under zero gravity at a rate of 11 lpm

and 1.7 also show the height predicted by the one-dimensional computational method of Thomas et al. [7]. The one-dimensional solution gave a nearly linear rise in the film height, whereas the two-dimensional solution is curved. The difference between the two solutions is within 10 percent. It can be recalled here that the two-dimensional solution is obtained by successive reduction in the rate of penetration and the final film height distribution approached a streamline, which is an essential characteristic of the free surface.

The distribution of velocity vectors for flow under zero gravity at a rate of 7 LPM is demonstrated in Fig. 1.8. The velocity profile across the thickness of the film was parabolic at all locations. The magnitude of the velocity, however, decreased as the fluid moved downstream. No jump or separation of flow was encountered in a zero-gravity environment, and the flow remained supercritical from entrance to exit.

The distribution of Nusselt number for radially-spreading flow on a disk is shown in Fig. 1.9. The disk surface was maintained at a uniform temperature higher than the entering fluid temperature. The free surface was assumed to be adiabatic with no evaporation. The Nusselt number was calculated as $Nu = h\delta/k$, where $h = q_w/(T_w - T_b)$. The Nusselt number decreased rapidly near the entrance due to the development of the thermal boundary layer from a uniform temperature condition at the entrance. The development of this boundary layer was extremely rapid. In the absence of gravity, the Nusselt number approached a uniform asymptotic value after a short distance from the entrance. In this case, the effect of flow rate was evident only in the thermally developing region and was very small in

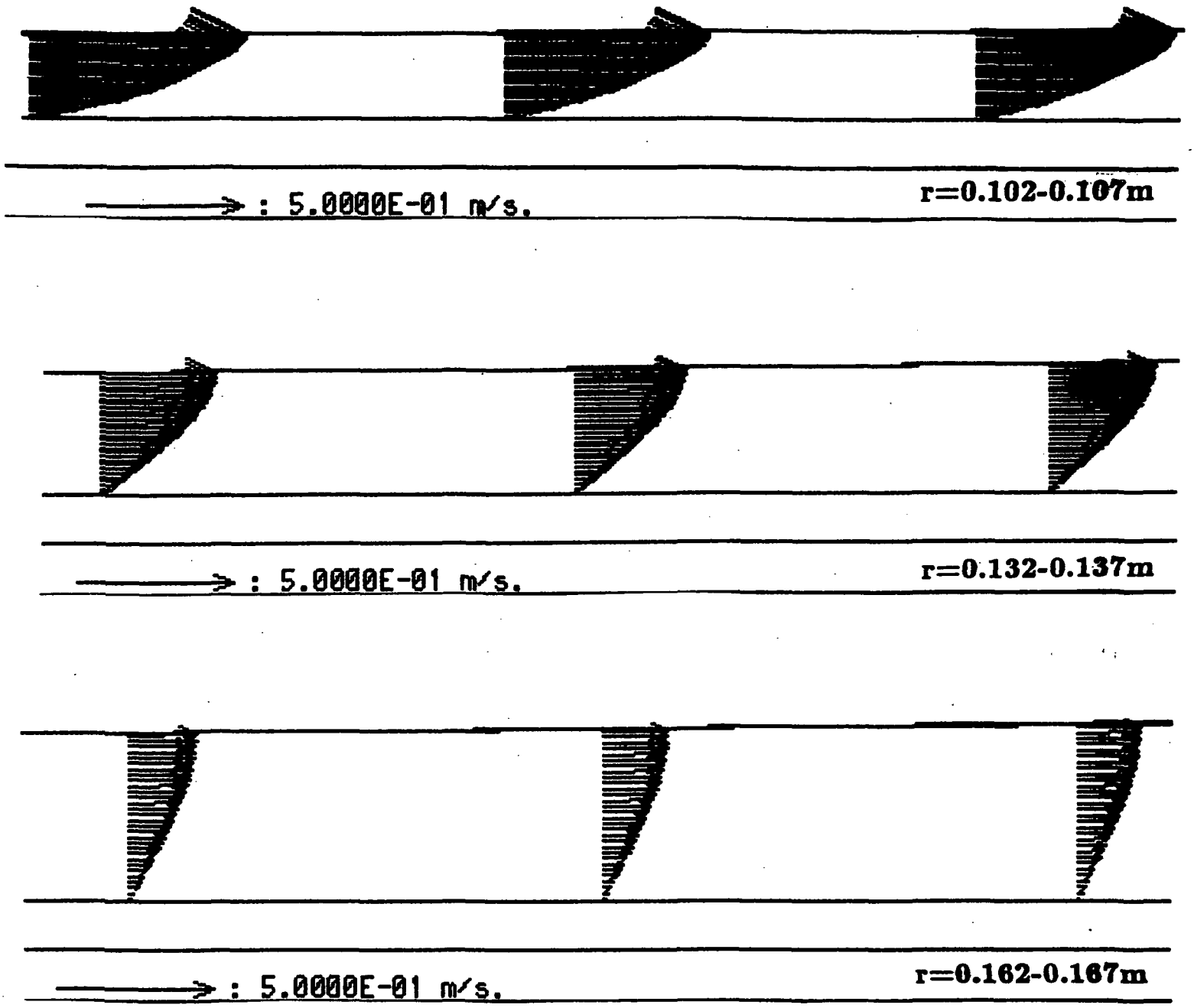

Fig. 1.8 Velocity vectors for radially spreading flow under zero gravity at a rate of 7 LPM

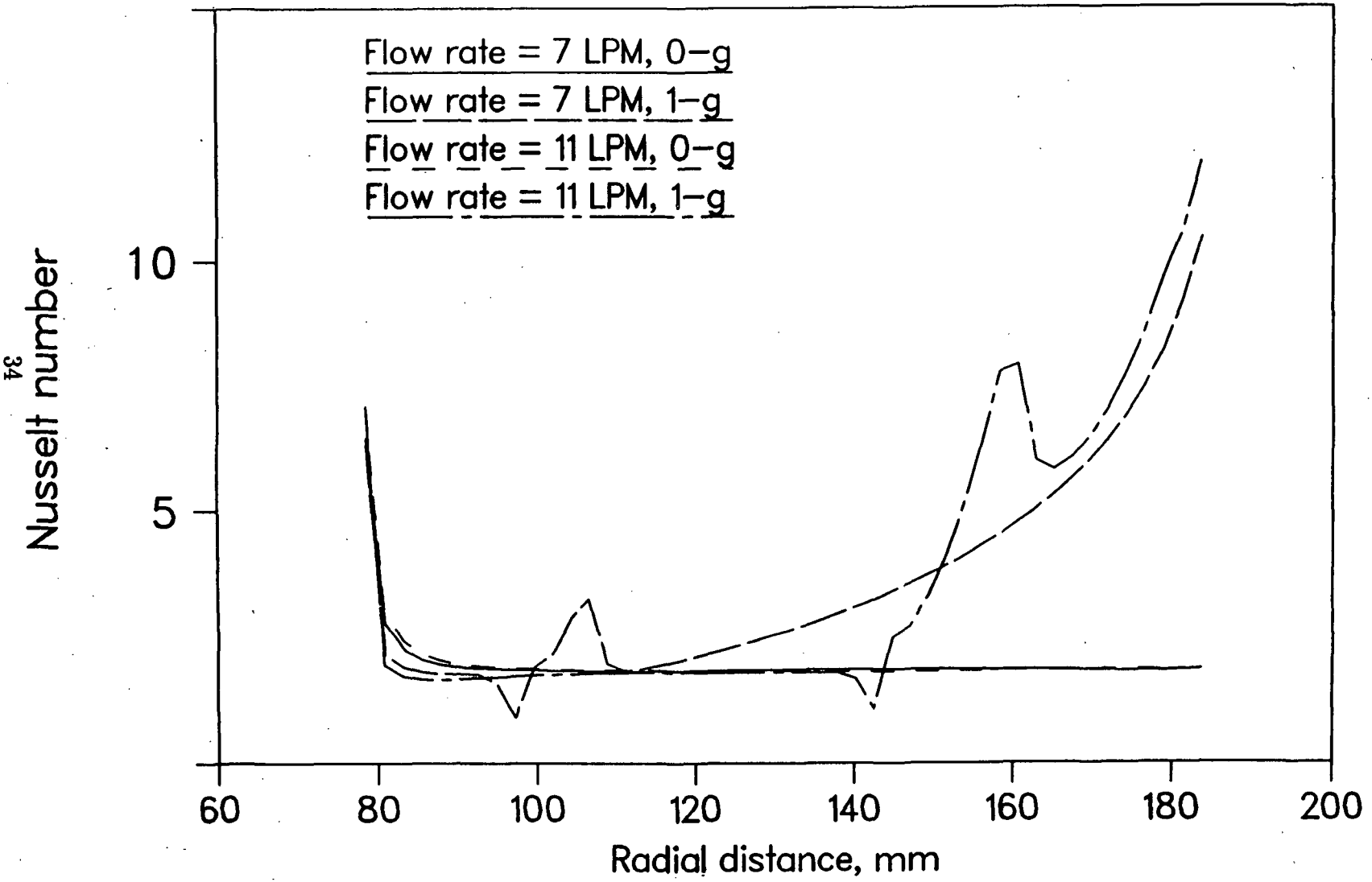

Fig.1.9 Distribution of Nusselt number in radially spreading flow

magnitude. The effect of flow rate became significant when gravity was present, since the hydraulic jump was encountered at different locations. In the supercritical region upstream from the jump, the Nusselt number approached a constant value following the development of thermal boundary layer. As soon as the jump was encountered, the Nusselt number first decreased, then increased to a peak, then decreased by a small amount, and increased monotonically further downstream. The irregular distribution in the vicinity of the jump is due to the churning motion of fluid and mixing of forward and recirculating flows. The monotonic increase in the subcritical region indicated the development of a thermal boundary layer in the recirculating flow region. The thickness of this boundary layer decreased with radius, and therefore, the Nusselt number increased. The maximum Nusselt number is seen to be at the exit end of the disk since the flow is forced to re-attach to the surface at that location due to the presence of the free falling liquid. Since the recirculating flow velocity was smaller than the main stream flow, the changes in the subcritical region were somewhat gradual in contrast to the rapid change in Nusselt number near the entrance. It can be recalled here that the film height, which was used as the lengthscale in the definition of the Nusselt number, was much larger in magnitude in the subcritical region than the supercritical region. To get a better understanding of the actual rate of heat transfer, the dimensional heat-transfer coefficient is presented in Fig. 1.10.

The heat-transfer coefficient decreased monotonically downstream in a zero-gravity environment. In contrast to the Nusselt number, the heat-transfer coefficient was found to be a function of flow rate, and as

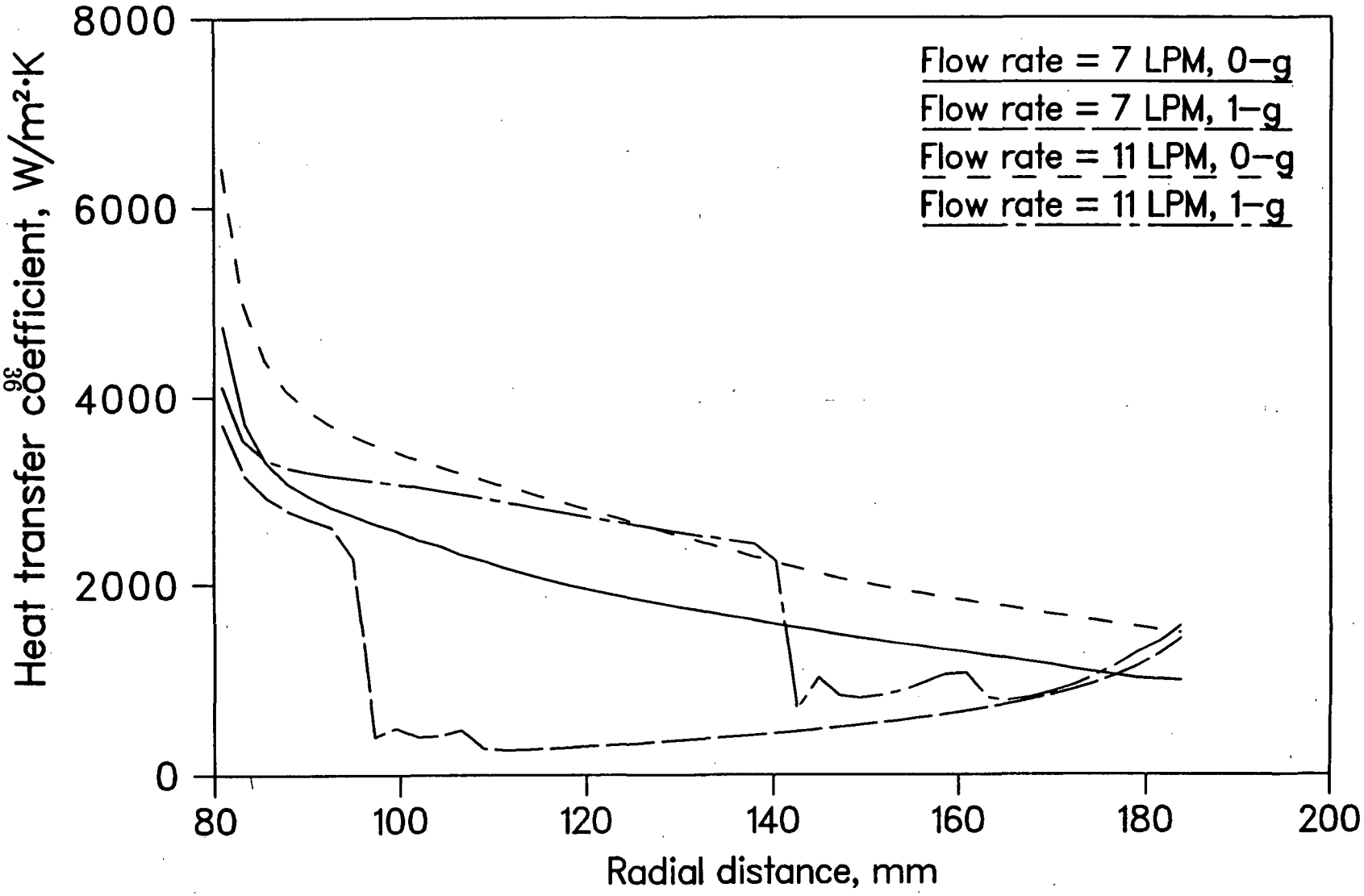

Fig.1.10 Distribution of local heat transfer coefficient in radially spreading flow

expected, the rate of heat transfer increased with flow rate. In the presence of gravity, the heat-transfer coefficient decreased gradually downstream in the supercritical region, attained a sudden drop as soon as the jump was encountered, went through a somewhat irregular distribution and then increased gradually in the subcritical region following the jump. The lower heat-transfer coefficient in the vicinity of the jump was expected, since the main flow in the supercritical region and the recirculating flow in the subcritical region gather hot fluid there, leading to a smaller wall to fluid temperature gradient. The irregular variation is possibly the result of the churning motion of fluid particles in the vicinity of the jump. For the flow rates and dimensions considered here, the average heat-transfer coefficient over the entire plate was larger for the zero gravity flow than the normal gravity flow. Therefore, a better cooling of the disk may be expected when the system is operated in a zero or reduced gravity environment, as in a space shuttle.

1.6 CONCLUSIONS

The computational methods for the prediction of the film height and heat-transfer coefficient of free surface flow of a thin liquid film adjacent to a stationary disk were critically investigated, significantly improved, and compared with experimental measurements. A model for estimating the film height at the outer edge of the disk when gravitational body force is present was developed. The 'pressure optimization method' was modified to appropriately handle flows involving a hydraulic jump. A new version of the 'porous wall method' was presented, where iterations are more systematic, uniformly convergent, faster, and yield more accurate results.

In the absence of gravity, the film height increased monotonically, and the heat-transfer coefficient decreased gradually downstream. In this case, the Nusselt number approached a constant value after the initial development of thermal boundary layer. The velocity profile across the thickness of the film was parabolic with the maximum at the free surface.

In the presence of gravity, a hydraulic jump was encountered that isolated the supercritical and subcritical flow regions. Flow separation was encountered at the location of the jump due to adverse pressure gradient and frictional resistance at the wall. The heat-transfer coefficient decreases downstream in the supercritical region and increases downstream in subcritical region with a sudden drop and fluctuations around the location of the jump. The predicted film height and location of the jump compared reasonably well with experimental measurements.

1.7 REFERENCES

1. E.J. Watson, The Radial Spread of a Liquid Jet over a Horizontal Plane, *J. Fluid Mechanics*, Vol. 20 Part 3, 481-499, 1964.

2. W.M. Kays and M.E. Crawford, *Convective Heat and Mass Transfer*, Second Edition, McGraw Hill, New York, 1980.

3. Z.H. Chaudhury, Heat Transfer in a Radial Liquid Jet, *J. Fluid Mechanics*, Vol. 20, Part 3, pp. 501-511, 1964.

4. T. Azuma and T. Hoshino, T., The Radial Flow of Thin Liquid Film, 1st through 4th Reports, *Bulletin of JSME*, Vol. 27, No. 234, pp. 2739-2770, 1984.

5. J. Stevens and B.W. Webb, Local Heat Transfer Coefficients Under an Axisymmetric, Single Phase Liquid Jet, to appear in *ASME J. Heat Transfer*, 1990.

6. J. Stevens and B.W. Webb, The Effect of Inclination on Local Heat Transfer Under an Axisymmetric, Free Liquid Jet, to appear in *Int. J. Heat Mass Transfer*, 1990.

7. S. Thomas, W. Hankey, A. Faghri and T. Swanson, One-Dimensional Analysis of the Hydrodynamic and Thermal Characteristics of Thin Film Flows Including the Hydraulic Jump and Rotation, *ASME J. Heat Transfer*, Vol. 112, No. 3, pp. 728-735, 1990.

8. S. Thomas, A. Faghri and W.L. Hankey, Experimental Analysis and Flow Visualization of a Thin Liquid Film on a Stationary and Rotating Disk, *ASME J. Fluids Engineering*, 1990, (in press).

9. M.M. Rahman, A. Faghri, W.L. Hankey and T.D. Swanson, Computation of the Free Surface Flow of a Thin Liquid Film at Zero and Normal Gravity, *Numerical Heat Transfer*, Part A., Vol. 17, pp. 53-71, 1990.

10. M.M. Rahman, A. Faghri and W.L. Hankey, New Methodology for the Computation of Heat Transfer Free Surface Flows Using a Permeable Wall, *Numerical Heat Transfer*, Part B, Vol. 18, pp. 23-41, 1990.

11. M.M. Rahman, A. Faghri, W.L. Hankey and T.D. Swanson, Prediction of Heat Transfer to a Thin Liquid Film in Plane and Radially Spreading Flows, *ASME J. Heat Transfer*, Vol. 112, No. 3, pp. 822-825, 1990.

12. D.A. Anderson, J.C. Tannehill and R.H Pletcher, *Computational Fluid Mechanics and Heat Transfer*, McGraw-Hill, New York, 1984.

13. S.V. Patankar, *Numerical Heat Transfer and Fluid Flow*, Hemisphere Publishing Corporation, N.Y., 1980.

14. D.B. Spalding, Mathematical Modeling of Fluid Mechanics, Heat Transfer and Chemical Reaction Processes, A Lecture Course, CFDU HTS/80/1, Imperical College, London, U.K., 1980.

15. M.M. Rahman, W.L. Hankey and A. Faghri, Analysis of Fluid Flow and Heat Transfer in a Thin Liquid Film in the Presence and Absence of Gravity, *Int. J. Heat Mass Transfer*, 1990, (in press).

16. V.E. Nakovyakov, B.G. Pokusaev and E.N. Troyan, Impingement of an Axisymmetric Liquid Jet on a Barrier, *Int. J. Heat Mass Transfer*, Vol. 21, pp. 1175-1184, 1978.

SECTION II

FLOW OVER A ROTATING DISK

2.1 SUMMARY

The results of a numerical simulation of the flow field and associated heat transfer coefficient are presented for the free surface flow of a thin liquid film adjacent to a horizontal rotating disk. The computation has been performed for different flow rates and rotational velocities using a three-dimensional boundary-fitted coordinate system. Since the geometry of the free surface is unknown and dependent on flow rate, rate of rotation and other parameters, an iterative procedure had to be used to ascertain its location. The computed film height agreed well with existing experimental measurements. The flow is found to be dominated by inertia near the entrance and close to the free surface and dominated by centrifugal force at larger radii and adjacent to the disk. The rotation enhances the heat transfer coefficient by a significant amount.

2.2 INTRODUCTION

The free surface flow of a thin liquid film adjacent to a rotating surface is an interesting fluid mechanics problem since a number of surface and body forces act on the system simultaneously to shape the flow structure. The most dominant of these forces are: the friction exerted by the disk; the centrifugal and Coriolis forces due to rotation of the disk; and the inertia from the incoming fluid stream. This kind of flow is also quite commonly encountered in engineering processes; e.g., evaporation or condensation on a turbine blade or spin coating of metals. The primary motivation of this study, however, is to understand the fluid flow and heat transfer in a proposed absorber unit for a space-based vapor absorption refrigeration system. This kind of system is expected to be very useful in a micro-gravity environment where the centrifugal body force can be an effective driving mechanism for the thinning of the film to promote the absorption of the refrigerant vapor into the absorbent.

The fluid motion adjacent to a rotating surface in an infinite quiescent fluid medium is one of the fundamental problems in viscous fluid flow. Sparrow and Gregg [1] presented an exact solution of the Navier-Stokes equation for this case by estimating the thickness of the boundary layer from a basic mass and momentum balance and developing a similarity variable to transform the partial differential equations for the conservation of mass and momentum to a set of ordinary differential equations. These equations were integrated numerically across the thickness of the boundary layer to determine radial, axial and tangential velocities in dimensionless form. Murthy [2] analyzed the effects of turbulence in this flow by using the integral method and compared the results with available experimental data.

In the present study, however, we are not concerned with boundary layer flow in an infinite medium of fluid, but flow of a thin film adjacent to a plate. The boundary layer, however, develops inside this thin liquid film and may extend all the way across the film. An analytical solution for the flow of a thin film adjacent to a rotating disk was presented by Rauscher et al. [3]. An asymptotic expansion technique was used where the radial spread of fluid was perturbed to determine the effects of convection, Coriolis acceleration, radial diffusion, surface curvature and surface tension. These higher-order effects were discussed on a physical basis. Their solution was valid for laminar flow with small Rossby number.

Espig and Hoyle [4] analytically studied the surface waves in a thin liquid layer on a rotating disk. Nusselt's equation for film thickness on an inclined plate was modified to develop an expression for average film thickness, taking into account the effects of rotation. The thickness was found to be a function of volumetric flow rate, fluid viscosity and angular velocity of the disk. Needham and Merkin [5] studied the development of non-linear waves on the surface of a horizontally rotating thin liquid film. Using an asymptotic expansion technique, they studied the flow of a film much smaller in thickness than the distance from the axis of rotation. This distance, in turn, was smaller compared to the total radius of the disk in order to eliminate any end effect. It was found that the thickness of the film changes rapidly near the entrance due to spreading, while further away from the inlet, the film height is mainly determined by the centrifugal force and viscous stress. An expressions for film thickness was presented, which appears to be the same as that developed by Espig and Hoyle [4].

The analysis of evaporation of a thin liquid film from a rotating surface was presented by Butuzov and Rifert [6]. A closed-form solution of the film thickness was derived by neglecting inertia and making a basic balance of centrifugal and frictional forces acting on the film. Bornside et al. [7] also studied evaporation from the free surface of a thin liquid film with reference to spin coating process. They developed a one-dimensional flow model accounting for variations of concentration, viscosity and diffusivity across the thickness of the spin coated film. The flow of the liquid was governed by a balance between centrifugal driving force and viscous resisting force. The equations of the flow and transport were solved using Galerkin finite element method.

In all the above-mentioned studies, the thin film was primarily driven by centrifugal force. The inertia of the incoming fluid was either negligible or assumed to be so. In a space-based absorption refrigeration system, however, the film is expected to be introduced at the center of the disk with a significant amount of inertia to have a continuous flow of absorbent on the disk. This kind of system, where liquid is introduced at the center of the disk from a pressurized container and driven both by inertial and centrifugal forces, was studied recently by Thomas et al. [8,9].

Thomas et al. [8] presented the numerical solution of the one-dimensional radial flow of a thin liquid film adjacent to a stationary and rotating disk. The continuity and momentum equations were integrated across the thickness of the film by assuming a flat velocity profile to develop a single equation for film velocity. The resistance to the flow due to wall shear stress was expressed in terms of an empirical friction coefficient which

was estimated from the radial flow velocity. The thickness of the film was predicted by solving the equation for film velocity as a transient problem using the MacCormack predictor-corrector method.

Thomas et al. [9] presented experimental measurements of radially spreading flow of a thin film adjacent to a horizontal disk. A non-obtrusive capacitance technique was used for the measurement of the film height distribution. A photographic study was done to understand the nature of the surface waves. Tests were performed both for stationary and rotating disks at flow rates ranging from 7 to 15 LPM. The rate of rotation varied between 0 and 300 RPM. Their experiments predicted the presence of a hydraulic jump when the disk was stationary. The jump moved downstream with an increase of the flow rate and rotational velocity. Waves were found to be present on the free surface at all flow rates and rates of rotation.

The present study is undertaken to develop a computational procedure for solving governing transport equations in their complete three-dimensional form for the flow of a thin liquid film adjacent to a rotating disk. This methodology elminated the need for assuming a friction coefficient as was done in the one-dimensional model developed by Thomas et al. [8]. Furthermore, an attempt is also made to improve the simple one-dimensional solution procedure. All computed results are compared with experimental measurements of Thomas et al. [10]. The details of the three-dimensional flow field and distribution of the heat-transfer coefficient are discussed.

2.3 MATHEMATICAL MODEL

The curvilinear boundary-fitted coordinate system used for the

three-dimensional numerical computation is shown in Fig. 2.1. The local coordinates are directed along lines connecting the centers of the adjacent grid cells. The x-axis is directed in the azimuthal direction, the y-axis perpendicular to the plate and the z-axis along the radial direction. The velocity components in these three directions are u, v and w, respectively. Due to the axisymmetric nature of the flow and vertical entrance and exit sections, u is directed parallel to the plate and v is directed perpendicular to the plate. However, the w-velocity changes its direction along the plate depending on the slope of the free surface. The height of the free surface from the solid wall is denoted by δ, which varies with radial location.

For incompressible flow with constant fluid properties, the equations for the conservation of mass, momentum, and energy are given by

$$\nabla \cdot \vec{V} = 0 \tag{2.1}$$

$$\frac{D\vec{V}}{Dt} = -\frac{1}{\rho}\nabla p + \nu\nabla^2 \vec{V} + \vec{g} \tag{2.2}$$

$$\frac{DT}{Dt} = \alpha\nabla^2 T \tag{2.3}$$

The terms due to viscous dissipation and pressure work in the energy equation are neglected as is typical for any low speed flow. Since the flow is symmetric about the axis of rotation, there was no variation of velocity or temperature in the angular direction, i.e. $\partial\vec{V}/\partial x = 0$ and $\partial T/\partial x = 0$. At the free surface, both tangential and normal stress components are zero. The vanishing tangential stress condition is represented by the zero velocity

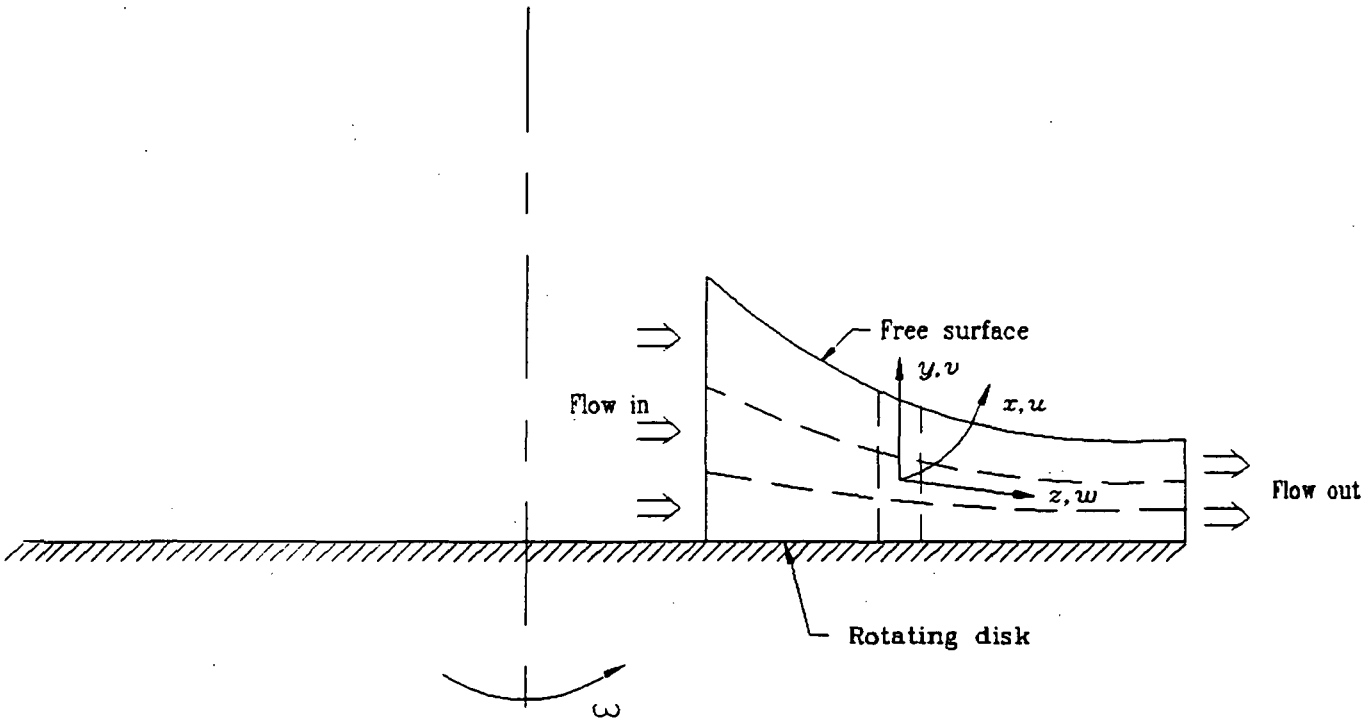

Fig.2.1 Schematic of the flow of a thin liquid film adjacent to a rotating disk

gradient on the free surface. The normal stress condition on the free surface leads to equations balancing the pressure and other stresses, including surface tension. Scaling these equations, one can show that, for a thin film flow where Weber and Reynolds numbers are large, all other stress terms are negligible compared to pressure, leading to $p = p_o$ on the free surface. The kinematic condition on the free surface relates the variation of film height to the velocity components. At the entrance plane, the velocity is assumed to be radial with a parabolic profile. At the exit plane, the flow is assumed to be fully developed with a hydrostatic pressure profile. The boundary conditions for the flow considered here are then given by

$$\text{at } y = 0: \quad \vec{V} = \omega r \vec{i}, \quad T = T_w \tag{2.4}$$

$$\text{at } y = \delta: \quad \frac{\partial \vec{V}}{\partial n} = 0, \quad p = p_o, \quad \frac{d\delta}{dz} = \frac{v}{w}, \quad \begin{cases} \frac{\partial T}{\partial n} = 0, & \text{heating} \\ T = T_{sat}, & \text{evaporation} \end{cases} \tag{2.5}$$

$$\text{at } z = r_{in}: \quad \vec{V} = W_{in} \left[2 \left(\frac{y}{\delta}\right) - \left(\frac{y}{\delta}\right)^2\right] \vec{k}, \quad T = T_{in} \tag{2.6}$$

$$\text{at } z = r_{out}: \quad \frac{\partial \vec{V}}{\partial z} = 0, \quad p = p_o + \rho g (\delta - y), \quad \frac{\partial T}{\partial z} = 0 \tag{2.7}$$

Here n is the direction normal to the free surface. The quantities T_w, T_{sat}, T_{in}, W_{in} and ω are assumed to be constant. Two different thermal conditions are considered on the free surface: simple heating without evaporation; and evaporation. For the first case, the free surface is assumed

to be adiabatic in nature. In the second case, the free surface is isothermal at its equilibrium saturation temperature, T_{sat}. In the present investigation, it is also assumed that, in the case of evaporation, the fluid enters at its equilibrium saturation temperature, i.e., $T_{in} = T_{sat}$. The Nusselt number is defined in terms of film thickness since that is the most significant length scale for this problem.

2.4 COMPUTATIONAL PROCEDURE

2.4.1 Three-Dimensional Method

The governing transport equations along with the boundary conditions described in the previous section were solved numerically using a boundary-fitted curvilinear coordinate system. The irregular free surface was taken as one of the boundaries of the computational domain. The solution domain had a pie shape structure extending from r_{in} to r_{out} in the radial direction and over a small angle in the angular direction in order to prevent both distortion of body-fitted coordinates at large radii and clustering of grids at smaller radii. The grid cells were generated by an algebraic interpolation between the boundaries of the domain. In general, the cell faces were non-orthogonal to each other. As shown in Fig. 2.1, the local coordinates were defined along lines connecting the centers of the adjacent grid cells. The x-axis was taken in the azimuthal direction, the y-axis perpendicular to the plate and the z-axis in the radial flow direction. The velocity resolutes in these three directions are u, v, and w, respectively. In the finite-difference formulation, the co-variant components, i.e., components parallel to the cell faces, were used to represent the velocity and force vectors.

The finite-difference equations were derived by using the principle of conservation of mass, momentum and energy at each cell. The primary variables were preserved in the formulation instead of doing any non-dimensionalization. The quantities were stored in a staggered fashion where they made more physical sense for cell conservation. For each cell, the velocity components were stored at downstream boundaries, whereas all pressures and temperatures were stored at the cell center. The mass flux across a cell boundary was computed exactly from the scalar product of the velocity vector and the vector representing the area of the cell face. The convection contribution to a cell from its neighbors were calculated exactly by taking into account the curvature of a cell face and its non-orthogonal orientation. In the calculation of diffusion, however, the cell boundaries were approximated to be locally orthogonal. The hybrid difference scheme, demonstrated by Patankar [10] was used to preserve the relative contribution of convection and diffusion to a cell from its neighbor in terms of cell Peclet number. This is a common practice in the computation of convective flows.

The distribution of cells in the computational domain was determined from a series of tests with different number of cells in the x, y, and z directions. Due to the axisymmetric nature of the flow, only 5 cells with an angular extent of 2.3°/cell were found to be adequate in that direction. This provided a total angle of 11.5° for the entire computation domain. Test runs with 3.45°/cell and 2.3°/cell yielded heat transfer coefficient within 0.001 percent. Similarly, runs with 2 cells and 5 cells in the angular direction gave heat transfer coefficient within 0.0005 percent. Similar tests for the other two directions showed that 50 cells in the radial direction and 30 cells across the thickness of the film results in grid-independent solutions.

Therefore, the computation domain was divided into 5 x 30 x 50 cells by simple algebraic interpolation to generate a uniformly distributed grid structure.

The finite difference equations were solved by using the SIMPLEST algorithm as presented by Spalding [11], which is an iterative solution procedure where the computation was started by guessing a value for the pressure. Then the momentum equations were solved to determine the velocity components. The pressure was updated using the continuity equation. Even though the continuity equation does not contain any pressure, it can be easily transformed to a pressure correction equation as shown by Patankar [10]. The iterations were continued until the sum of the residuals for all computational cells dropped below 10^{-6} for each equation. Since the flow was not coupled to the thermal transport for the problem considered here, the temperature field was solved once the film height distribution was completely ascertained.

Since the geometry of the free surface was dependent on the flow parameters, but needed to be specified to generate the grid structure for the three-dimensional computation, an iterative procedure had to be used to ascertain the location of the free surface. The free surface boundary was assumed to be a permeable wall through which fluid particles were allowed to enter or leave the computational domain. Since the ambient pressure was prescribed, an outflow took place when the static pressure of the fluid adjacent to the free surface was higher than the ambient pressure and vice versa. The penetration of fluid through the free surface essentially violated the kinematic condition on the surface, which was arrived at by adjusting the surface height distribution in successive iterations. The scheme worked as follows:

1. A free surface height distribution was prescribed (based on one-dimensional solution of Thomas et al. [8] or any improved method.

2. The flow field was solved completely for that height distribution.

3. The amount of penetration of the fluid through the surface was calculated at all location along the flow.

$$(Q_{loss})_k = Q_{k-1} - Q_k$$

4. The new free surface height was determined from the old height and the rate of penetration.

$$(\delta_{new})_k = (\delta_{old})_k + a \frac{(Q_{loss})_k}{Q_{in}} (\delta_{old})_k$$

where a is the relaxation factor.

5. Iterations were continued until the rate of penetration became negligible.

For a given surface height distribution, the deviation from the ideal zero penetration condition was estimated by the following measures.

(a) Root square penetration

$$= \frac{\sqrt{\sum_{k=1}^{n} (Q_{loss})_k^2}}{Q_{in}} \qquad (2.8a)$$

(b) Absolute sum of penetration

$$= \frac{\sum_{k=1}^{n} |(Q_{loss})_k|}{Q_{in}} \qquad (2.8b)$$

(c) Maximum error in flow rate

$$= \frac{|(Q - Q_{in})|_{max}}{Q_{in}} \qquad (2.8c)$$

All these quantities were found to decrease almost monotonically with iterations. The final results presented here had both absolute sum of penetration and maximum error in flowrate of less than 0.06 and root square penetration less than 0.02. A relaxatim factor of α = 1 was found to be adequate in most computations. Since flow field was not affected by thermal transport, the energy equation was solved only for the final free surface height distribution with no penetration through the surface. The above computational algorithm is termed as porous wall method originally outlined by Rahman et al. [12]. Significant modifications of the method, however, have been made here to improve the iteration procedure as well as the error estimates. Moreover, this is the first time it has been applied to predict the three-dimensional flow involving rotation.

2.4.2 Improved One-Dimensional Method

The one-dimensional computational procedure, developed by Thomas et al. [8] was also improved here by incorporating a better estimate of frictional resistance exerted by the solid wall on the flow. In the one-dimensional method, the governing equations for mass and momentum were integrated across the thickness of the film assuming a uniform velocity profile. In the

original procedure of Thomas et al. [8], the flow was assumed to be strictly radial in nature with a superimposed solid-body rotation. The resistance to the flow due friction was taken to be the resistance in the radial direction. In the azimuthal direction, the velocity remained constant across the thickness of the film with no resistance form the solid wall. In reality, however, the velocity is expected to change due to the finite viscosity of the fluid, so there will be frictional resistance form the wall in the azimuthal direction. To account for the frictional resistance due to the angular velocity, we may define the total shear stress as

$$\tau_w = \sqrt{\tau_\phi^2 + \tau_r^2} \qquad (2.9)$$

Here $\tau_r = c_f\ (1/2\ \rho\ W^2)$, where c_f can be calculated by using the Blasius (see Kays and Crawford [13]) or parabolic solution given by Rahman et al. [14]. Also, τ_ϕ can be estimated from the exact solution of laminar flow adjacent to a rotating disk in an infinite extent of fluid. As given by Schlichting [15],

$$\tau_\phi = 0.6\ \rho r\ {}_v 1/2\ {}_\omega 3/2 \qquad (2.10)$$

Using τ_w as the shear stress at the solid wall, the discretized equations of Thomas et al. [8] were reformulated and solved to give the film height distribution for any given flowrate and rate of rotation.

2.5 RESULTS AND DISCUSSION

The three-dimensional computational procedure discussed in the previous section was first tested against the limiting flow situations, where

theoretical or experimental results are already available. By setting the rotational speed to zero, the computed results reproduced exactly the film height distribution and velocity field corresponding to two-dimensional thin film flow adjacent to a stationary disk as presented by Rahman et al. [12]. Another limiting case was the flow motion induced by a rotating disk in an otherwise stagnant infinite fluid stream. Analytical solutions for this case was developed by Sparrow and Gregg [1]. In this system, the flow is limited to a thin boundary layer adjacent to the disk. The computed solution for this limiting case was plotted in Fig. 2.2, where it was compared with the analytical results of Sparrow and Gregg [1]. The non-dimensional distance, ζ, and velocity components G and F are defined as

$$\zeta = y \sqrt{\frac{\omega}{\nu}} \tag{2.13}$$

$$F = \frac{w}{r\omega} \tag{2.14}$$

$$G = \frac{u}{r\omega} \tag{2.15}$$

It can been seen that both the radial and azimuthal velocity distributions across the thickness of the boundary layer are reasonably matched. One major difference between the conventional boundary layer flow and the flow of a thin film is that the thickness of the film is finite and bounded by the free surface which interacts with the surrounding medium.

The height of a thin film adjacent to a rotating disk was experimentally measured by Thomas et al. [11]. A horizontal disk of diameter 406.4 mm was

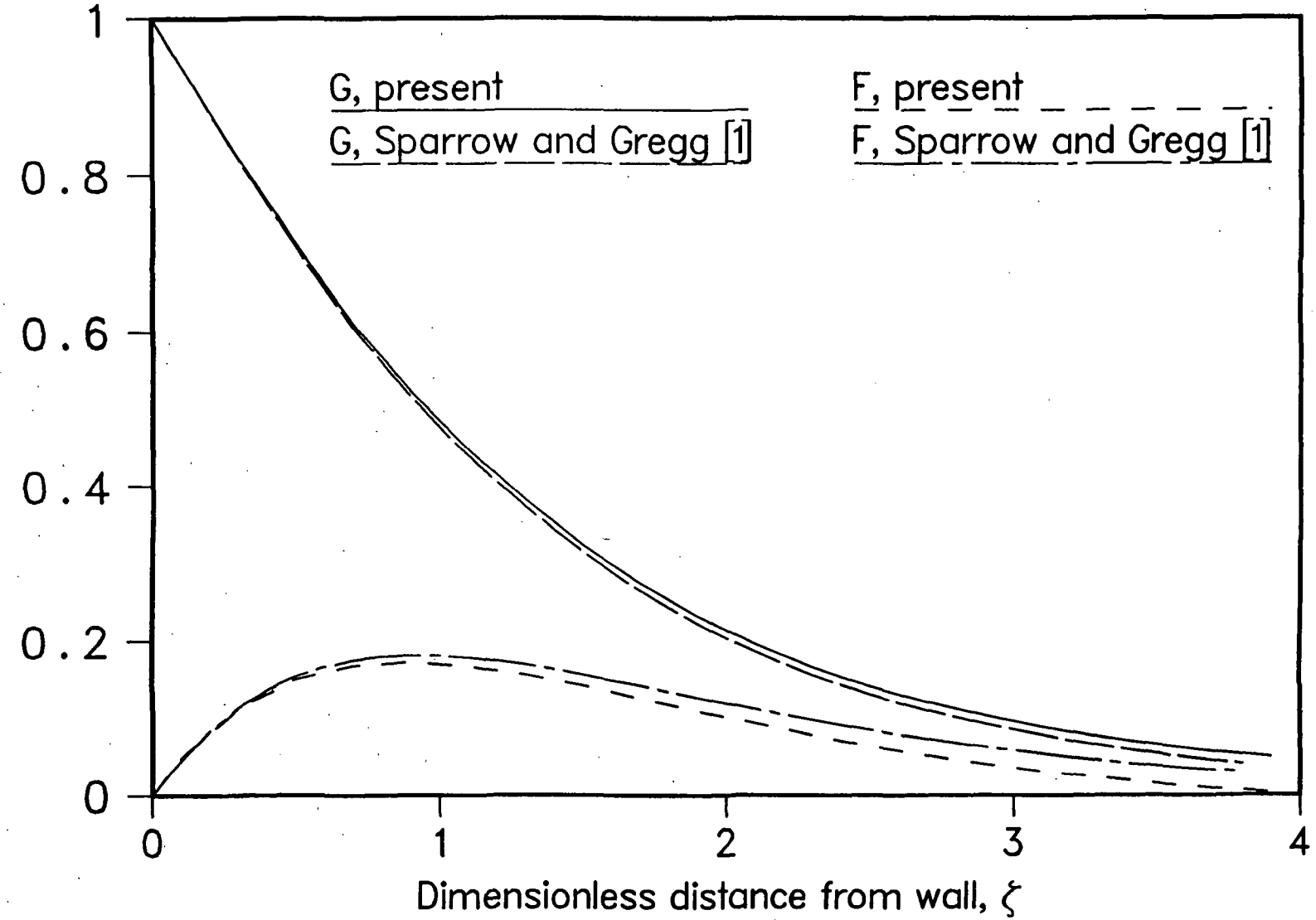

Fig.22 Comparison of numerical results with similarity solution for fluid motion adjacent to a rotating disk in infinite fluid medium

used for the experiment where water at 20^{o}C was introduced radially through a slot of height 0.267 mm at a radial location of 50.8 mm. The film height was measured by using a non-obstrusive capacitance probe from 76.2 mm to 195.6 mm. The measurements were not reported past 195.6 mm because part of the capacitance sensor was over the edge of the disk. Twenty sets of experimental data were taken covering flow rates of 7-15 LPM and rotational speeds of 55-300 RPM. The flow was isothermal and no measurement of heat transfer was done in that experiment. In the present investigation, we used the flow and rotation conditions presented by Thomas et al. [11], so that a relative comparison of the film height distribution could be made. The specific cases chosen here are listed in Table 2.1. Prediction of film height and heat transfer coefficient could be done for all the experimental runs. However, to save the compuational efforts, some specific cases were picked up to cover the range of experiment in terms of flow rate and rate of rotation, as well as to understand the trend of variation of flow field and heat transfer coefficient with flow rate and rotational speed. The table also lists the root square penetration, absolute sum of penetration and maximum error in flow rate corresponding to the three-dimensional film height distribution for each specific flow rate and rate of rotation. For computational runs involving heat transfer, the wall temperature is assumed to be 30^{o}C, whereas the entering fluid (water) is at 10^{o}C. This gives a film temperature of 20^{o}C for the evaluation of properties.

The computed film height for a flow rate of 9 LPM and rotational speed of 200 RPM (case 1 in Table 2.1) is shown in Fig. 2.3. The experimental data as well as the computed results using previous one-dimensional solution algorithms are also shown in the same figure. It can be noticed that the

Table 2.1

Flow and Rotation Rates in Present Investigation

Case #	Flow Rate (LPM)	Rotational Speed (RPM)	Root Square Penetration	Absolute Sum of Penetration	Maximum Error in Flow Rate
1	9	200	0.0043	0.0199	0.0113
2	15	200	0.0072	0.0235	0.0152
3	7	100	0.0050	0.0258	0.0152
4	11	100	0.0110	0.0406	0.0218
5	15	300	0.0020	0.0097	0.0076
6	15	55	0.0127	0.0593	0.0540
7	7	300	0.0148	0.0445	0.0100
8	15	100	0.0092	0.0332	0.0224

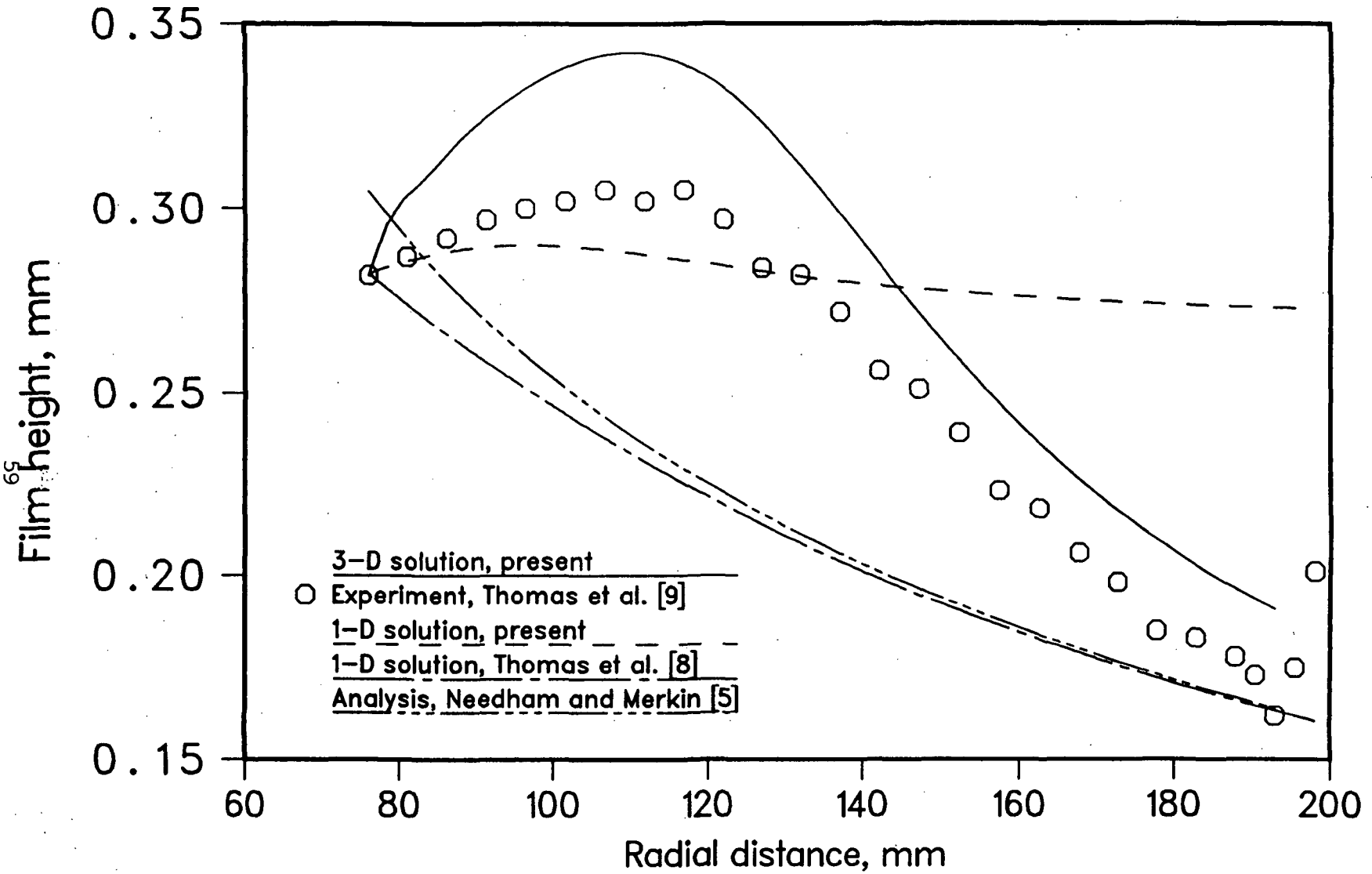

Fig.23 Comparison of numerical solution with experimental data for thin liquid film at a flow rate of 9 LPM and angular velocity of 200 RPM

three-dimensional solution predicts the trend of the experimental data, i.e., the film height first increases, attains a peak and then decreases further downstream. The increase of the film height near the entrance is due to strong frictional resistance the flow encounters from the solid wall. However, as the radius increases, the centrifugal force increases in magnitude and overpowers the frictional resistance. Then the film height decreases due to the increase in flow velocity as well as radial spreading. This latter effect is more significant at smaller radii. At larger radii, the curvature decreases and radially spreading flow approaches a plane flow. The one-dimensional solution of Thomas et al. [8] shows a monotonic decrease of film height with radius, and the height is consistently underpredicted except very close to the exit. Thomas et al. [8] assumed a solid-body rotation condition with no variation of velocity across the thickness of the film. Moreover, friction was computed based on the radial velocity using an empirical correlation. Therefore, the centrifugal force was more and frictional force was less accounted for in the numerical formulation. Therefore, the trend seen here is quite expected. The modified one-dimensional solution presented here improved the prediction of film height at smaller radii, but failed to do so at large radii. Here both radial and azimuthal components of frictional forces were accounted for, but still keeping no velocity variation across the thickness of the film. It may be noticed that the present three-dimensional solution, unlike the one-dimensional methods, does not require any estimate of friction coefficient. Figure 2.3 also shows a comparison with the analysis of Needham and Merkin [5]. Since the analysis presented an asymptotic solution valid for solid-body rotation, the analytical solution shows a monotic decrease in film height and compares well with the computation of Thomas et al. [8], where

similar assumptions were incorporated. In reality, however, viscous resistance at the wall slow down the film and result in a larger height distribution. Moreover, the asymptotic solution neglects the effects of inertia which was significant in the experiment and adequately taken care of in the three-dimensional solution. The computed results for a rotational rate of 200 RPM and flow rate of 15 LPM (case 2 in Table 2.1) are shown in Fig. 2.4. Here, the present three-dimensional solution gives a very good agreement with the experimental data. The one-dimensional algorithm of Thomas et al. [8] consistently underpredicts the film height whereas the solution present one-dimensional algorithm improves it somewhat, particularly near the entrance and exit. The analytical solution of Needham and Merkin [5] shows a large film height near the entrance that monotonically decreases downstream. Near the entrance, the flow is dominated by inertia, and therefore, the analytical results of Needham and Merkin [5] is not valid in that region.

The film height at a rotation rate of 100 RPM for two different flow rates (cases 3 and 4 in Table 2.1) are shown in Figs. 2.5 and 2.6. It can be seen that at this rate of rotation, the one-dimensional solution procedure using resultant frictional resistance gives a reasonable overall agreement, whereas the procedure of Thomas et al. [8] still underpredicts the film height at most locations. The analytical solution, as before, overpredicts the film height at smaller radii and underpredicts it at larger radii. The present three-dimensional solution gives the best agreement with the experimental data even though it does not coincide with it. A small overestimate of the film height near the entrance may be because of the development of the velocity profile from the given entrance boundary condition. At this boundary, the velocity was assumed to be parabolic in nature with a maximum on the free

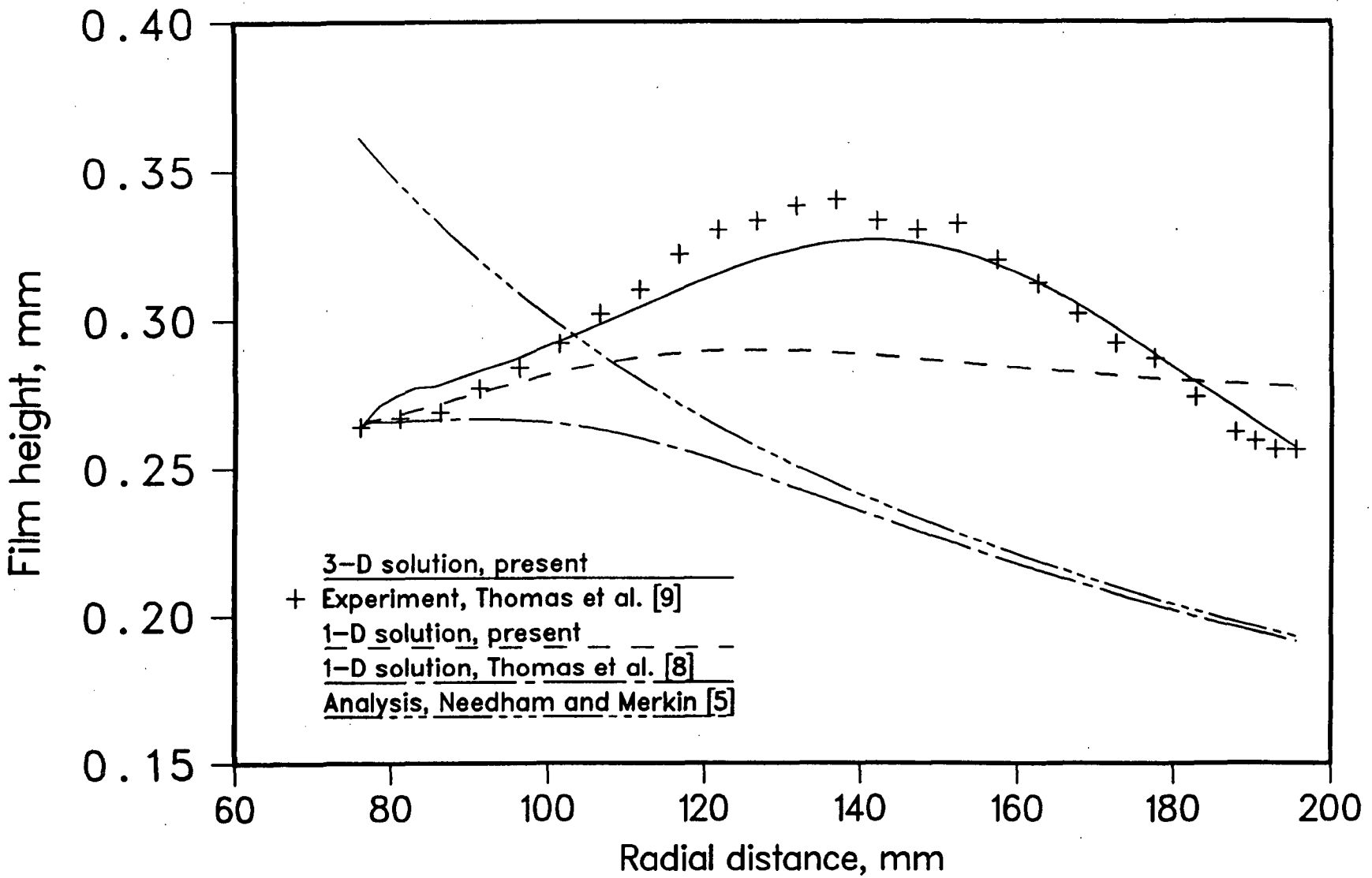

Fig.24 Comparison of numerical solution with experimental data for thin liquid film at a flow rate of 15 LPM and angular velocity of 200 RPM

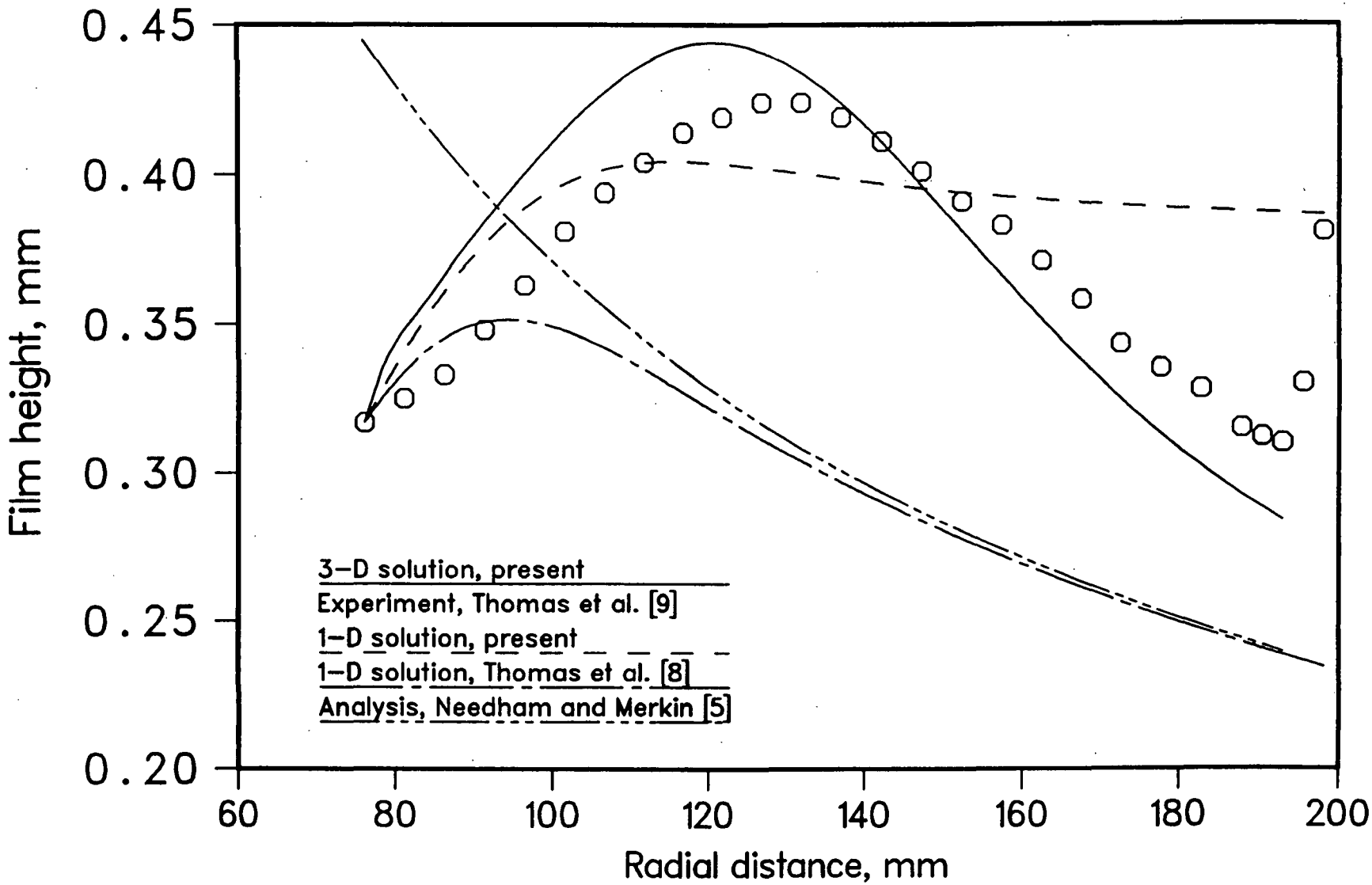

Fig.25 Comparison of numerical solution with experimental data for thin liquid film at a flow rate of 7 LPM and angular velocity of 100 RPM

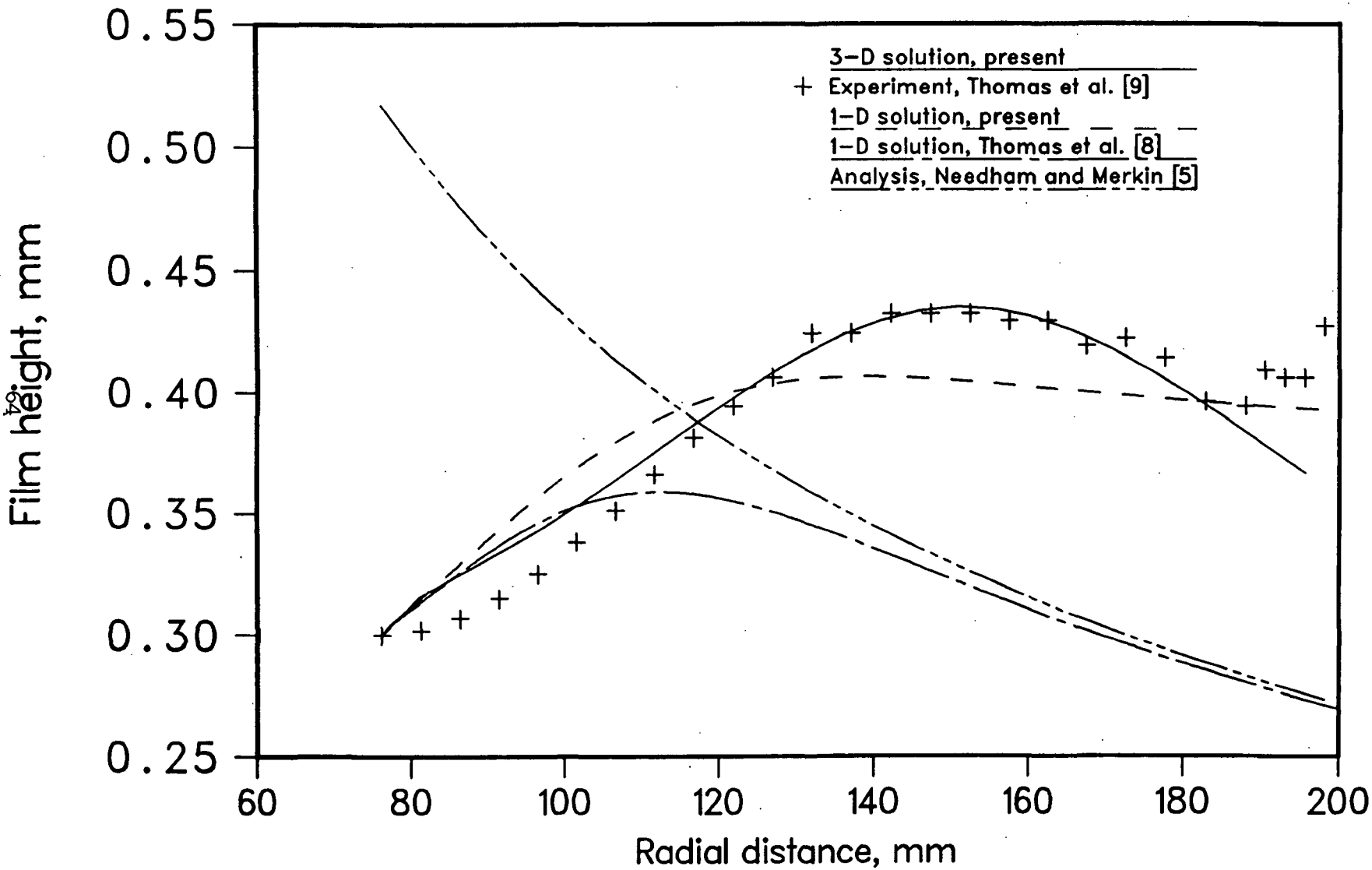

Fig.2.6 Comparison of numerical solution with experimental data for thin liquid film at a flow rate of 11 LPM and angular velocity of 100 RPM

surface. This is the best condition one can impose, particularly for laminar flow, as confirmed from the distribution of velocity across the thickness of the film in an intermediate location of the flow.

The distribution of the film height for 300 RPM and flow rate of 15 LPM (case 5 in Table 2.1) is shown in Fig. 2.7, where it is compared with the one-dimensional predictions of Thomas et al. [8] experimental data of Thomas et al. [9] as well as the analysis of Needham and Merkin [5]. In this situation, the numerical solution underpredicts the experimental data in most regions. The one-dimensional algorithm of Thomas et al. [8] produces a film height distribution that is much smaller than the experimentally measured values. The present one-dimension algorithm improves it further, whereas, the present three-dimensional solution compares best with the experimental data. The trend of the data that the film height first increases, attains a peak and then decreases downstream is only captured by the present three-dimensional numerical solution. The one-dimensional solutions for this case show a monotonic decrease of film height with radius. It may be noticed here that analysis of Needham and Merkin [5] compares better with the computation of Thomas et al. [8] at a larger rate of rotation since the effects of inertia become smaller. The above comparisons (Figs. 2.3-2.7) show that the present algorithm can be an effective means for the prediction of the film height for a thin film flow adjacent to a rotating disk. The small deviations from the experimental values are within the uncertainties of experimental measurements and can also be attributed to unsteady surface waves as well as the surface tension effects that were not accounted for in the present steady-state numerical formulation, especially at the outer edge of the disk where the film height suddenly increased.

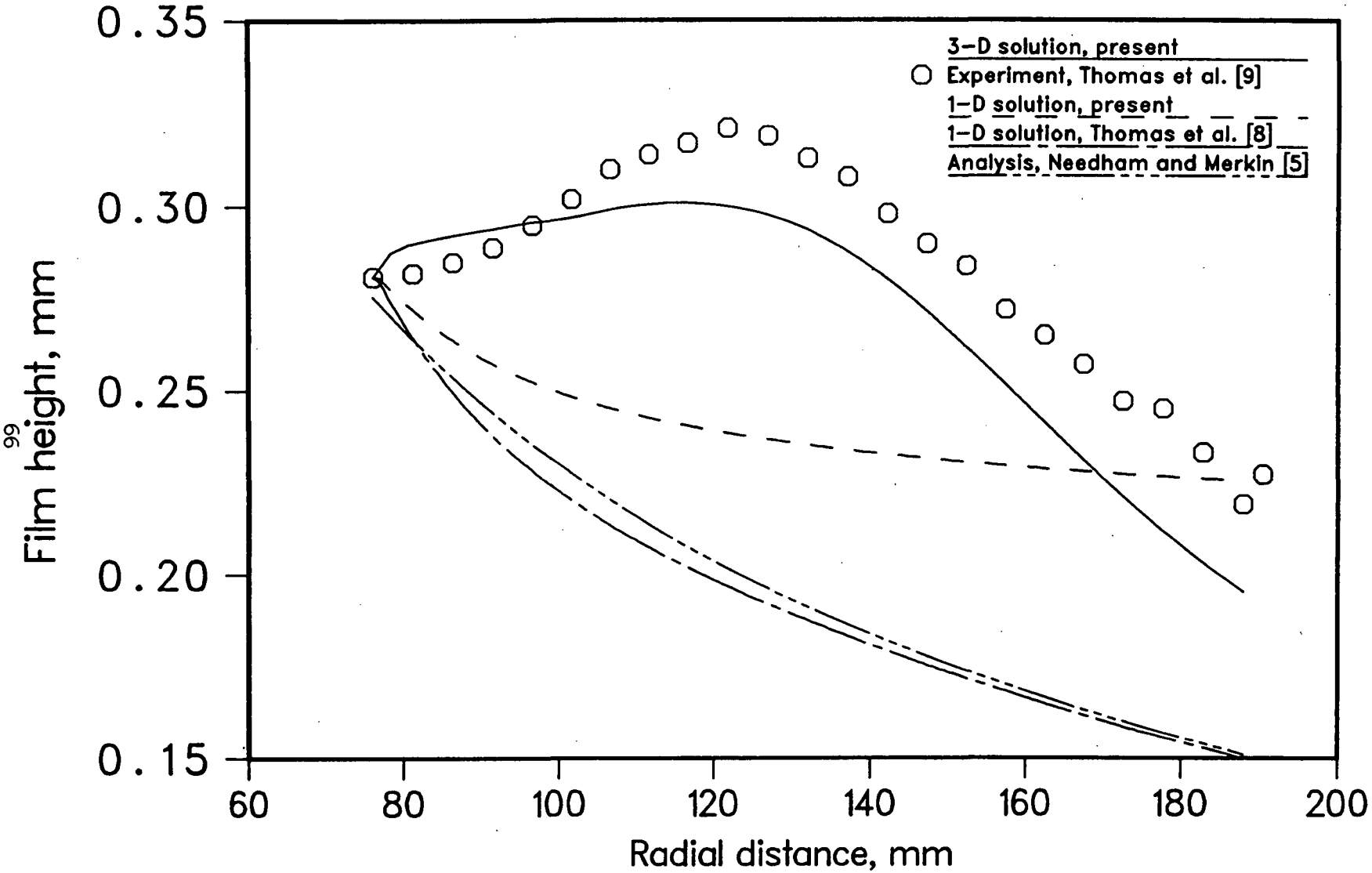

Fig2.7 Comparison of numerical solution with experimental data for thin liquid film at a flow rate of 15 LPM and angular velocity of 300 RPM

The distribution of the velocity vectors at three locations across the film are shown in Figs. 2.8 and 2.9, respectively, for two limiting operating conditions: case 6 (55 RPM, 15 LPM) and case 7 (300 RPM, 7 LPM). In Fig. 2.8, it can be seen that the velocity was almost radial at $y/\delta = 0.88$. Since the flow rate was high compared to the rate of rotation, the flow near the free surface was almost radial at this condition. At $y/\delta = 0.13$, which was near the solid wall, it can be seen that the velocity vectors were directed more in the angular direction, particularly at larger radii. Looking at the magnitude of the velocity vectors, it can be seen that the centrifugal force increases as the radius increases. At $y/\delta = 0.48$, it can be seen that the velocity vectors turn at an angle that increases with radial distance. Also, the overall magnitude of the vectors decreases with radius due to the resistance exerted by the solid wall. The flow is dominated by inertia at smaller radii and at locations away from the wall, whereas the contribution of rotation becomes important at locations near the solid wall and in regions away from the center. From a plot of the velocity components in the radial and azimuthal directions, it was found that the w-velocity profile is approximately parabolic in nature with a maximum at the free surface and zero at the wall. This corroborates corresponding observations for a stationary disk as presented by Rahman et al. [12]. The azimuthal component is maximum at the solid wall and gradually decreases as the free surface is approached. The normal component of velocity was found to be small compared to either of these components.

In Fig. 2.9, it can be noticed that the flow is dominated by rotation in most regions except near the entrance when the rotational speed is 300 RPM and flow rate is 7 LPM. At this condition, the inertia is overpowered by the high

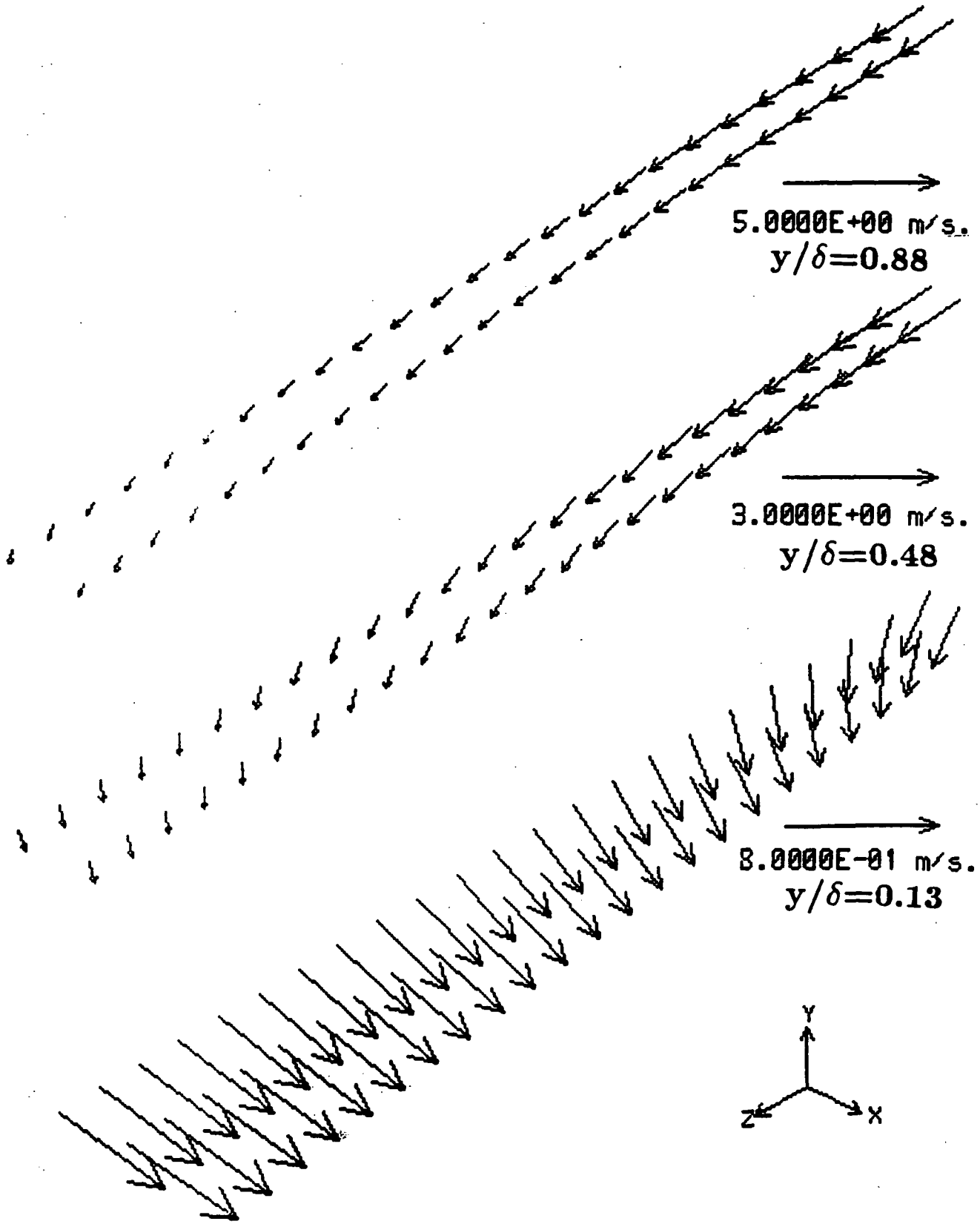

Fig.28 Velocity vectors for thin liquid film at a flow rate of 15 LPM and angular velocity of 55 RPM

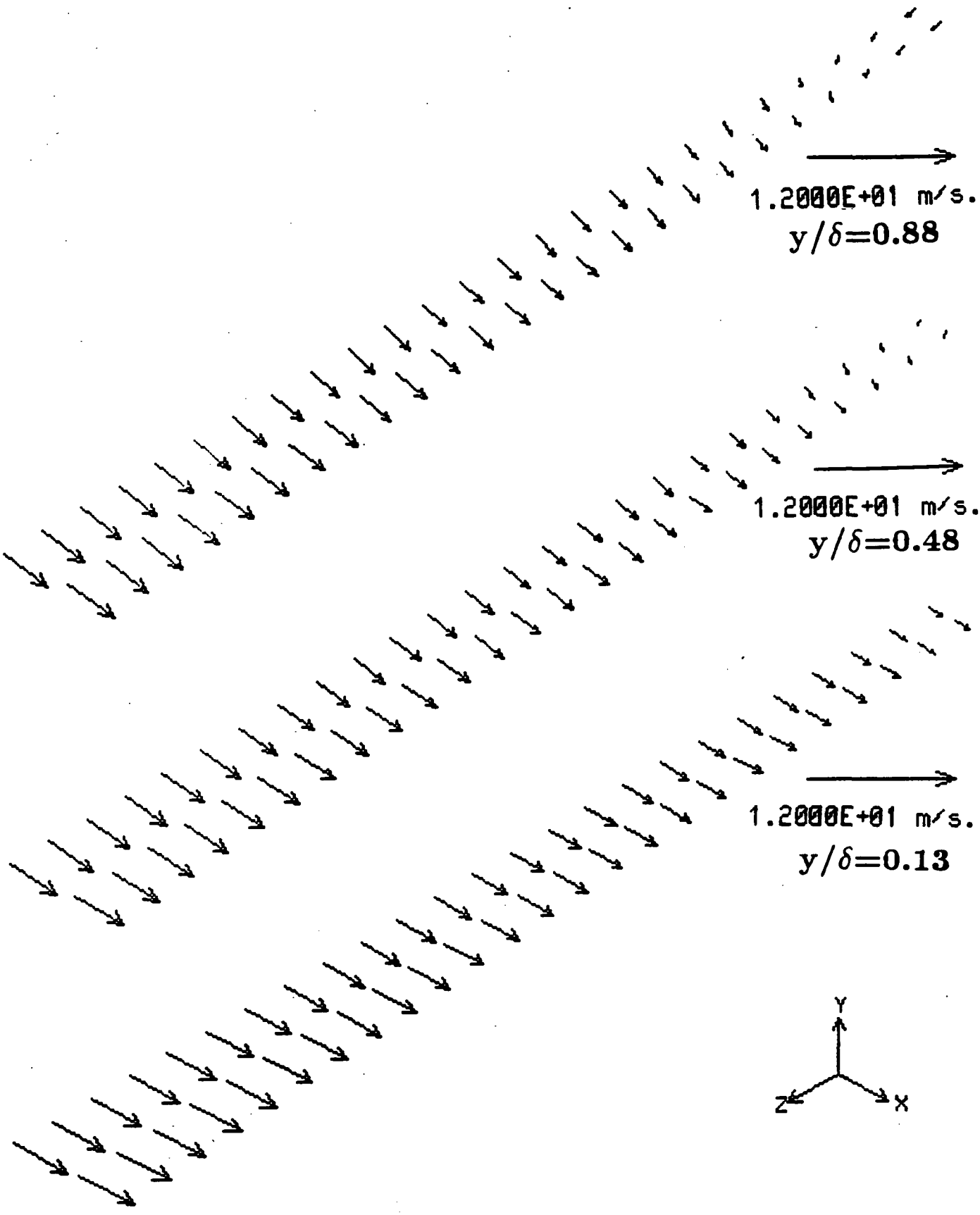

Fig.2.9 Velocity vectors for thin liquid film at a flow rate of 7 LPM and angular velocity of 300 RPM

rotational velocity after traversing some distance. Looking at the magnitude, it can also be noticed that the resultant velocity increases with radius. At intermediate conditions, the vector plots showed behavior within these two limits. The effect of the flow rate was found to increase the radial component of velocity, whereas rotation increased both radial and azimuthal components. The friction always counteracts these velocities to arrive at an equilibrium. The fluid particles exit the disk at an angle with the radial direction that increases with the rate of rotation.

A plot of Nusselt number for a flow rate of 15 LPM at two different rates of rotation are shown in Fig. 2.10 (cases 5 and 8 in Table 2.1). The plots correspond to two different thermal boundary conditions on the free surface, namely, simple heating without evaporation, when the free surface is approximately adiabatic in nature, and evaporative free surface when the surface is isothermal at the equilibrium saturation temperature. The thermal condition at the rotating disk surface is assumed to be a uniform temperature higher than the entering fluid (or saturation) temperature. It can be seen that the Nusselt number decreases rapidly near the entrance at all flow and heating conditions. This is due to the development of the thermal boundary layer as the fluid moves downstream. For both the cases of heating and evaporation, it can be seen that the Nusselt number for the case of 300 RPM decreases monotonically all the way to the exit, whereas in the case of 100 RPM, the Nusselt number decreases first, attains a minimum and then increases further downstream to approach an approximately constant value near the exit. The Nusselt number for heating is consistently found to be higher than the corresponding case of evaporation at all radial locations and all rates of rotation. This is also observed in connection with heat transfer to a falling

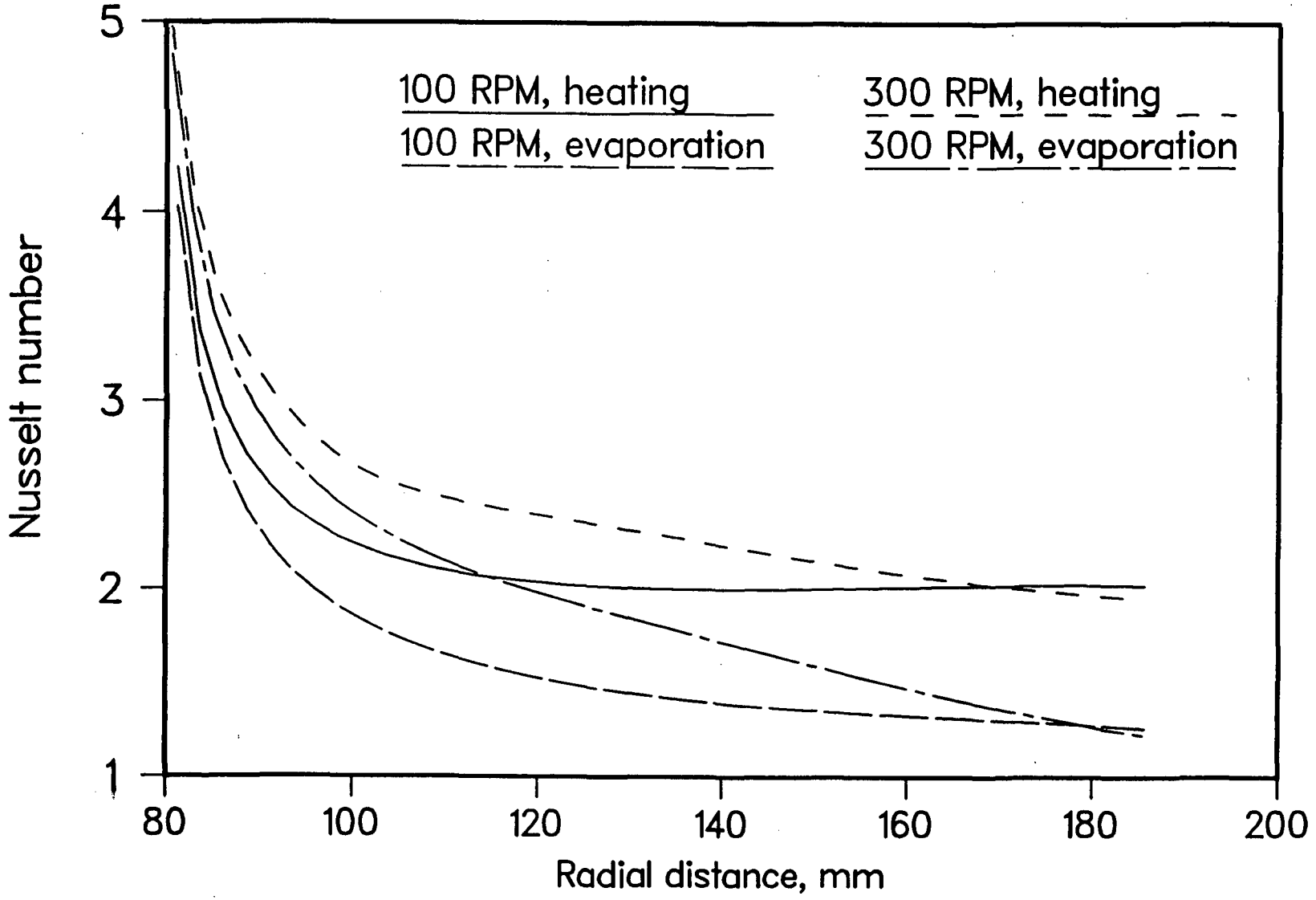

Fig.2.10 Nusselt number distribution for thin liquid film at a flow rate of 15 LPM

liquid film presented by Seban and Faghri [16]. The Nusselt number for 300 RPM is found to be higher than that for 100 RPM in most regions of the disk except close to the exit. The slightly higher Nusselt number near the exit is due to much larger film height than the corresponding case of 300 RPM. From this figure it can also be seen that an overall enhancement of Nusselt number is obtained by increasing the rate of rotation.

The Nusselt number here is defined in terms of local film thickness, which also varies along the radius. The film thickness also decreases as the rotational velocity increases. To see the distribution of the heat-transfer rate more clearly, the values of the heat-transfer coefficient for the same flow rate and heating conditions are shown in Fig. 2.11. It can be seen that heat-transfer coefficient for 300 RPM is consistently higher than that for 100 RPM at all radial locations. This is quite expected since the rate of rotation increases the centrifugal force which accelerates and thins the film, both of which contribute to the enhancement of heat transfer. It can also be seen that for the case of 300 RPM and simple heating, the heat transfer coefficient decreases near the entrance, attains a minimum and then increases further downstream. For the other cases shown here, the heat transfer coefficient approaches approximately a constant value after gradual decrease near the entrance. As the radius increases, the inertial force decreases and centrifugal force increases, both of which are counteracted by frictional resistance at the solid wall. In the absence of rotation or any external body force, the heat-transfer coefficient gradually decreases downstream as seen in the studies by Rahman et al. [12] for radial flow at zero gravity. The rotation balances out or even overcomes the frictional resistance at larger rate of rotation, as seen in the vector plot for 300 RPM (Fig. 2.9).

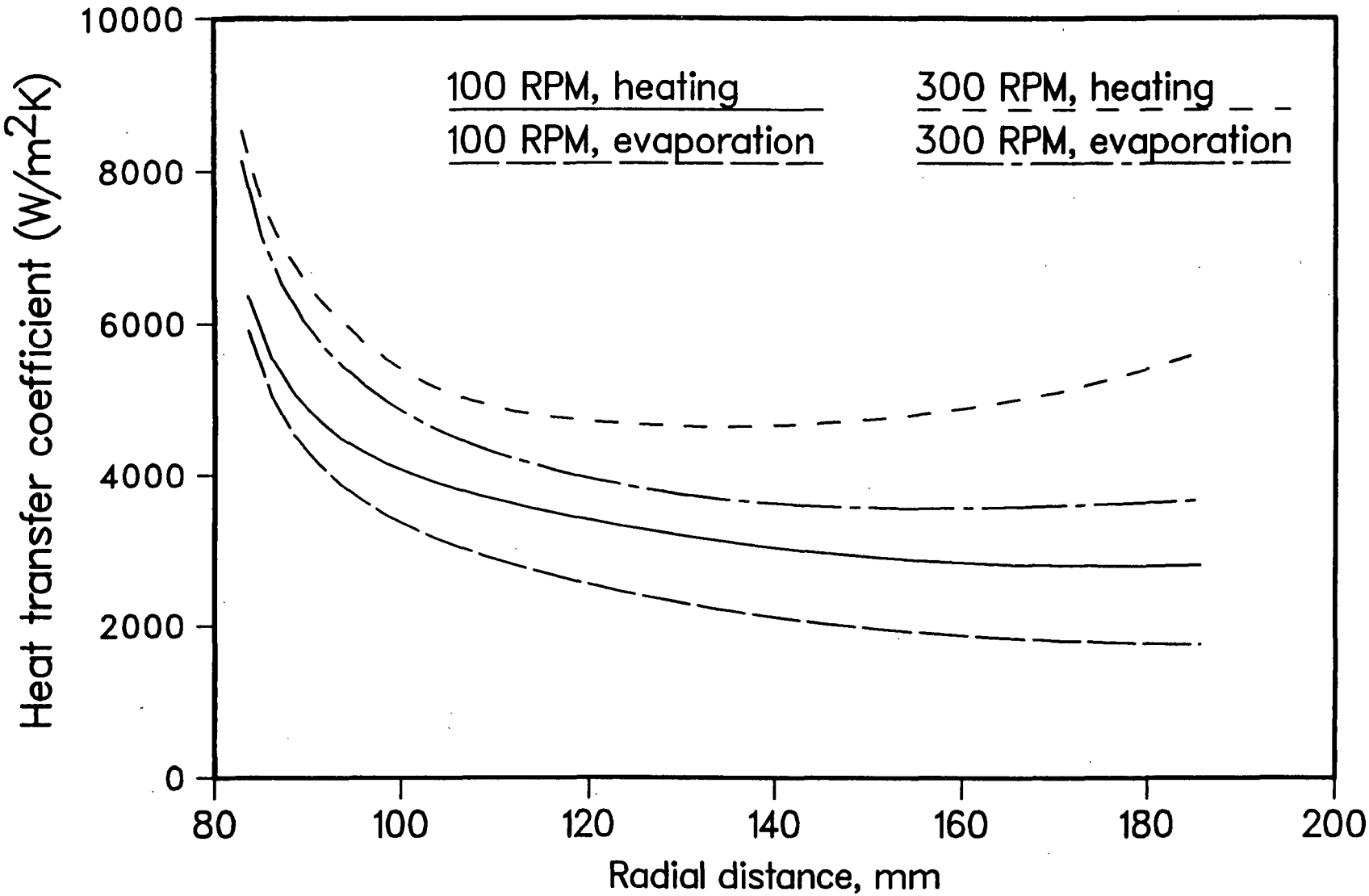

Fig.2.11 Heat transfer coefficient for thin liquid film at a flow rate of 15 LPM

Therefore, the convective heat transfer, which is intimately related to the fluid velocity, increases downstream once the centrifugal force becomes the dominant driving mechanism. If a disk of larger radius was considered, we could possibly see a minimum followed by a gradual rise in the heat-transfer coefficient for all cases. It can also be noticed that the effects of rotation in the enhancement of the heat-transfer coefficient is more for the case of simple heating than the case of evaporation.

Figure 2.12 shows the variation of Nusselt number with radial distance for a given rate of rotation at different flow rates. For the case of 15 LPM, the Nusselt number monotonically decreases from the entrance radius, but for the case of 7 LPM, it decreases gradually at smaller radii and approaches a constant value further downstream. The behavior is the same for both the cases of heating and evaporation. For the disk considered here, the Nusselt number for 15 LPM is found to be higher than that for 7 LPM at all radial locations. This is expected, particularly at smaller radial locations, since fluid velocity will be higher at larger flow rates. At large radii, however, when effects of rotation become more important, a higher heat-transfer coefficient may be attained by using a smaller flow rate due to more thinning of the film. So, by controlling the disk radius, flow rate and rate of rotation, one may attain any desired requirement of heat transfer in this kind of flow system.

2.6 CONCLUSIONS

Numerically computed distributions of the film height, velocity vectors and heat-transfer coefficient are presented for the free surface flow of a thin liquid film adjacent to a horizontal rotating disk. The flow is found to

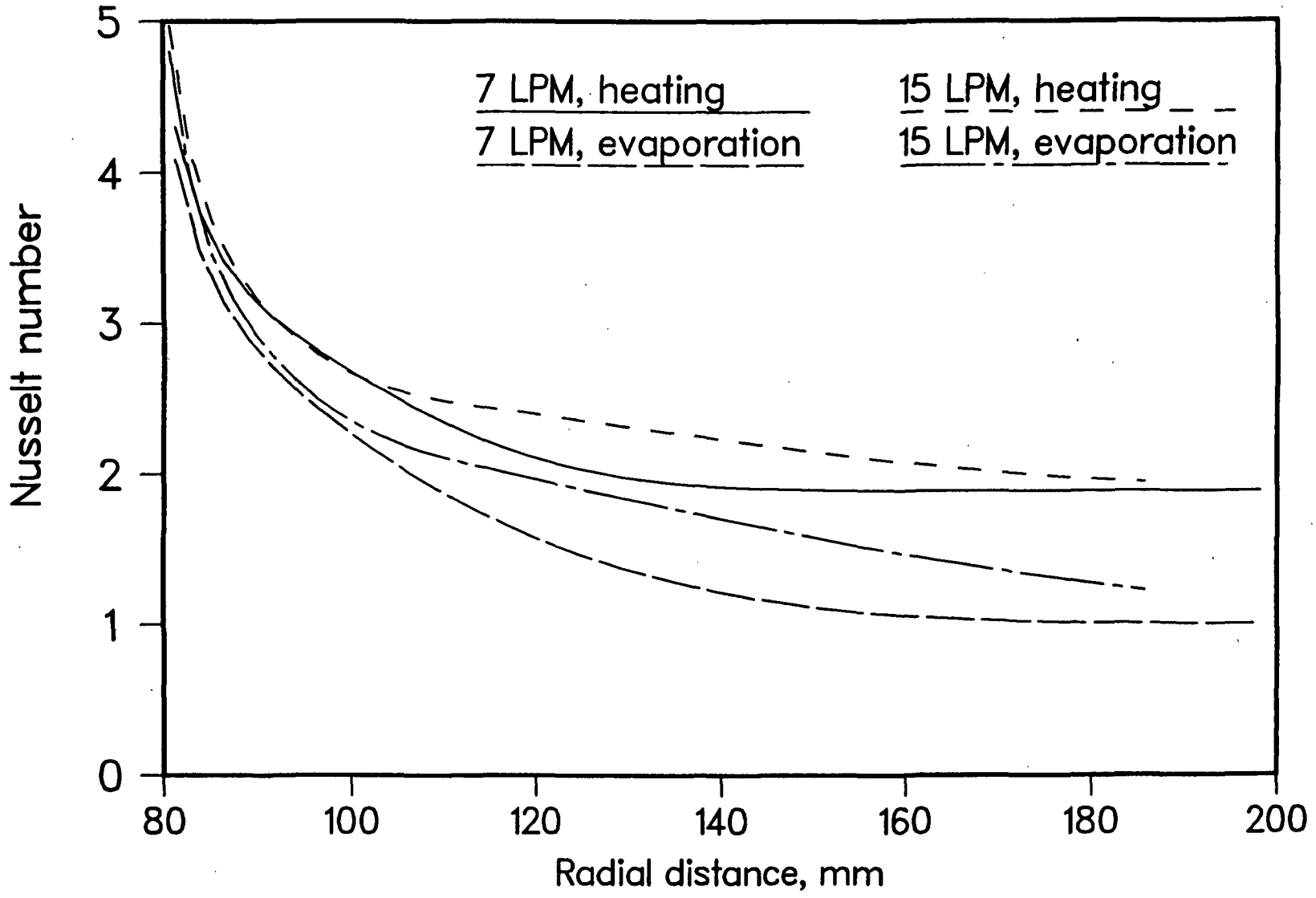

Fig.2.12 Nusselt number distribution for thin liquid film at a rotation rate of 300 RPM

be dominated by inertia at smaller radii and close to the free surface and dominated by rotation near the solid wall and at larger radii. The radial component of velocity is found to have an approximately parabolic profile which is maximum at the free surface and zero at the solid wall. The angular component of velocity is maximum at the wall and gradually diminishes across the thickness of the film. The local fluid velocity is increased with an increase in both the volumetric flow rate and angular velocity of rotation. The fluid particles exit the disk at an angle with radius that increases with rate of rotation. At the flow rates and rates of rotation considered here, the film height first increases, attains a peak and then decreases further downstream. The increment of the film height is attributed to frictional resistance whereas the reduction of the film height at larger radii is due to the spreading of the film as the flow area increases as well as the increase of the centrifugal force with radius. The predicted height using the present three-dimensional computational method agreed well with experimental measurements. The rate of heat transfer is enhanced by a significant amount by increasing the rate of rotation for both the cases of simple heating with no evaporation and evaporation at the free surface.

2.7 REFERENCES

1. E.M. Sparrow and J.L. Gregg, Mass Transfer, Flow and Heat Transfer About a Rotating Disk, *ASME J. Heat Transfer*, **82**, 294-302 (1960).

2. V.N.D. Murthy, Combined Laminar and Turbulent Flow Over a Rotating Disk, *Indian J. Technology*, **14**, 107-112 (1976).

3. J.W. Rauscher, R.E. Kelly and J.D. Cole, An Asymptotic Solution for the Laminar Flow of a Thin Film on a Rotating Disk, *ASME J. Applied Mechanics*, **40(1)**,43-47 (1973).

4. H. Espig and R. Hoyle, Waves in Thin Liquid Layer on a Rotating Disk, *J. Fluid Mechanics*, **22(4)**, 671-677 (1965).

5. D.J. Needham and J.H. Merkin, The Development of Nonlinear waves on the surface of a Horizontally Rotating Thin Liquid Film, *J. Fluid Mechanics*, **184**, 357-379 (1987).

6. A.I. Butuzov and V.G. Rifert, Heat Transfer in Evaporation of Liquid From a Film on a Rotating Disk, *Heat Transfer-Soviet Research*, **5(1)**, 57-61 (1973).

7. D.E. Bornside, C.W. Macosko and L.E. Scriven, Spin Coating: One-Dimensional Model, *Journal of Applied Physics*, **66(11)**, 5186-5193 (1989).

8. S. Thomas, W.L. Hankey, A. Faghri and T. Swanson, One-Dimensional Analysis of the Hydrodynamic and Thermal Characteristics of Thin Film Flows Including the Hydraulic Jump and Rotation, *ASME J. Heat Transfer*, **112 (3)**, 728-735 (1990).

9. S. Thomas, A. Faghri and W.L. Hankey, Experimental Analysis and Flow Visualization of a Thin Liquid Film on a Stationary and Rotating Disk, to appear in *ASME J. Fluids Engineering*, (1990).

10. S.V. Patankar, *Numerical Heat Transfer and Fluid Flow*, Hemisphere Publishing Corporation, N.Y. (1980).

11. D.B. Spalding, Mathematical Modeling of Fluid Mechanics, Heat Transfer and Chemical Reaction Processes, A Lecture Course, CFDU HTS/80/1, Imperial College, London. (1980).

12. M.M. Rahman, A. Faghri, and W.L. Hankey, New Methodology for the Computation of Heat Transfer in Free Surface Flows Using a Permeable Wall, *Numerical Heat Transfer*, Part B., **18 (1)**, 23-41 (1990).

13. W.M. Kays and M.E. Crawford, *Convective Heat and Mass Transfer*, Second Edition, McGraw Hill, N.Y. (1980).

14. M.M. Rahman, W.L. Hankey and A. Faghri, Analysis of Fluid Flow and Heat Transfer in a Thin Liquid Film in the Presence and Absence of Gravity, *Int. J. Heat Mass Transfer*, (1990) (in press).

15. H. Schlichting, *Boundary Layer Theory*, Seventh Edition, McGraw Hill, N.Y. (1979).

16. R.A. Seban and A. Faghri, Evaportion and Heating with Turbulent Falling Liquid Films, *ASME J. Heat Transfer*, **98 (2)**, 315-318 (1976).